universe

MDPI

Article

New Sources of Leptonic CP Violation at the DUNE Neutrino Experiment

Alessio Giarnetti and Davide Meloni *

Dipartimento di Matematica e Fisica, Università di Roma Tre, Via della Vasca Navale 84, 00146 Rome, Italy; alessio.giarnetti@uniroma3.it
* Correspondence: davide.meloni@uniroma3.it

Abstract: We check the capability of the DUNE neutrino experiment to detect new sources of leptonic CP violation beside the single phase expected in the Standard Model. We illustrate our strategy based on the measurement of CP asymmetries in the case that new physics will show up as nonstandard neutrino interactions and sterile neutrino states and show that the most promising one, once the experimental errors are taken into account in both scenarios, is the one related to the $\nu_\mu \to \nu_e$ transition.

Keywords: neutrino physics; new physics; CP violation

check for updates

Citation: Giarnetti, A.; Meloni, D. New Sources of Leptonic CP Violation at the DUNE Neutrino Experiment. *Universe* **2021**, *7*, 240. https://doi.org/10.3390/universe7070240

Academic Editor: Ricardo G. Landim

Received: 3 June 2021
Accepted: 2 July 2021
Published: 12 July 2021

Publisher's Note: MDPI stays neutral with regard to jurisdictional claims in published maps and institutional affiliations.

Copyright: © 2021 by the authors. Licensee MDPI, Basel, Switzerland. This article is an open access article distributed under the terms and conditions of the Creative Commons Attribution (CC BY) license (https://creativecommons.org/licenses/by/4.0/).

1. Introduction

Neutrino flavor oscillations are one of the most important particle physics discoveries of the last several decades [1]. Experiments using natural and artificial neutrino sources were able to measure mixing parameters with a good precision [2,3]. In particular, the three mixing angles, as well as the absolute values of the mass splittings, were determined with a small percentage of uncertainty. However, some degeneracies still exist and future experiments should aim to solve them. In particular, the atmospheric mass splitting sign (hierarchy problem) and the octant in which the atmospheric angle θ_{23} lies are still unknown. Moreover, the phase of the PMNS matrix, which is the only source of CP violation in neutrino oscillation, has not been measured with a satisfactory precision [4,5]. The other two phases appearing in the most general neutrino Lagrangian, in which both Majorana and Dirac mass terms are taken into account, do not affect the oscillation probabilities. Thus, they could only be tested using other phenomenon (i.e., neutrinoless double beta decay).

Even though most of the experimental results are in agreement with the three-neutrino paradigm, the longstanding short baseline [6–8] and reactor [9–12] anomalies gave some hint of new physics (NP) phenomena such as the presence of additional sterile neutrino states [13–24]. Moreover, uncertainties on the oscillation parameters leave rooms for the presence of additional effects in neutrino interaction [25–27] and propagation in matter not contemplated in the Standard Model (SM) and that which can be described in a model-independent way by four fermions effective operators, namely the nonstandard interactions (NSI) operators [28–39].

Both types of NP models introduce new sources of CP violation in neutrino oscillations. In particular, when one sterile state is contemplated, the 4×4 PMNS matrix contains two more phases than in the SM case. If we take the possibility that neutrinos can undergo NSI during their travel through matter into account, three new phases in the state evolution equations emerge.

The NP phases inevitably affect CP violation in neutrino oscillations, whose presence can be highlighted from CP-odd observables; among them, asymmetries of the type $A_{\alpha\beta} \sim P(\nu_\alpha \to \nu_\beta) - P(\bar{\nu}_\alpha \to \bar{\nu}_\beta)$ can be directly measured with future neutrino experiments capable of distinguishing neutrino from antineutrino events. Such quantities are generally

dependent on the CP phases and become a smoking gun for new CP violation as soon as their values deviate from the SM predictions, including matter effects [40].

The goal of the present paper is to test whether neutrino experiments will perform sufficiently well as to establish that other phases beside the single one expected in the SM are responsible for CP violation in the lepton sector. To achieve our aim, we adopt the following strategy:

- compute the leptonic asymmetries in the SM;
- evaluate the experimental uncertainty on them;
- recompute the asymmetries including the effects of NP;
- check whether the new results are sufficiently away from the SM predictions.

The outcome of our procedure is the identification, if any, of the most promising asymmetry capable to produce an experimental signature well beyond the SM expectations.

We validate our strategy studying the asymmetries as they can be measured at the Deep Underground Neutrino Experiment (DUNE) [41–44]. An unprecedented feature of DUNE will be the possibility to study three different transition channels (namely $\nu_\mu \to \nu_\mu$, $\nu_\mu \to \nu_e$, $\nu_\mu \to \nu_\tau$) and the neutral current (NC) neutrino interactions using both neutrino and antineutrino fluxes; thus, this experiment will be able to measure four independent asymmetries.

The manuscript is organized as follows. In Section 2, we discuss the analytic structure of the relevant asymmetries in the SM, by means of the perturbation theory in the small parameters (to be defined later in the manuscript) and in the regime of small matter effects (a perfectly viable approximation for DUNE); we then repeat the same calculation in the NSI scenario (Section 3) and in the $3+1$ sterile neutrino model (Section 4). Section 5 is devoted to a description of the DUNE experiment and the impact of NP of the neutrino energy spectra. In Section 6, we show the foreseen experimental values on the asymmetries built in terms of number of events (integrated asymmetries) and their related uncertainties, both in the SM and in the NP scenarios. Eventually, in Section 7, we draw our conclusions. Expressions of the probabilities in the NP models analyzed here are provided in the Appendices A and B.

2. CP Asymmetries in the Standard Model

The neutrino state evolution equations when they travel through matter can be written as:

$$i\frac{d}{dt}\begin{pmatrix}\nu_e\\ \nu_\mu\\ \nu_\tau\end{pmatrix} = \left[\frac{1}{2E_\nu}U\begin{pmatrix}0 & 0 & 0\\ 0 & \Delta m^2_{21} & 0\\ 0 & 0 & \Delta m^2_{31}\end{pmatrix}U^\dagger + A_{CC}\begin{pmatrix}1 & 0 & 0\\ 0 & 0 & 0\\ 0 & 0 & 0\end{pmatrix}\right]\begin{pmatrix}\nu_e\\ \nu_\mu\\ \nu_\tau\end{pmatrix}, \quad (1)$$

where U is the usual neutrino mixing matrix and $A_{CC} \equiv \sqrt{2}G_F n_e$, with n_e being the electron density in the Earth crust. Defining $P(\nu_\alpha \to \nu_\beta)$ as the transition probability from a flavor α to a flavor β, one can construct the CP-odd asymmetries as:

$$A_{\alpha\beta} \equiv \frac{P(\nu_\alpha \to \nu_\beta) - P(\bar{\nu}_\alpha \to \bar{\nu}_\beta)}{P(\nu_\alpha \to \nu_\beta) + P(\bar{\nu}_\alpha \to \bar{\nu}_\beta)}\,. \quad (2)$$

It is well known that matter effects modify the behavior of the asymmetries as a function of the Standard Model CP phase δ (see, e.g., [45]): in fact, the passage of neutrinos through matter introduces fake CP-violating effects which allows $A_{\alpha\beta} \neq 0$ even when $\sin\delta = 0$. In principle, to extract genuine CP violating effects, one could define the subtracted asymmetries as $A^{\rm sub}_{\alpha\beta}(\delta) = A_{\alpha\beta}(\delta) - A_{\alpha\beta}(\delta = 0)$. However, we prefer to deal with more directly measurable quantities, and we will use Equation (2), which, for non-negligible matter effects, are nonvanishing when $\delta = 0, \pm\pi$.

To derive the analytic expressions for the asymmetries, we use perturbation theory in the small $\alpha = \Delta m^2_{21}/\Delta m^2_{31}$ ratio [26] and expand the mixing angles according to:

$$s_{13} = \frac{r}{\sqrt{2}}\,, \qquad s_{12} = \frac{1}{\sqrt{3}}(1+s)\,, \qquad s_{23} = \frac{1}{\sqrt{2}}(1+a)\,, \tag{3}$$

where r, s, and a represent the deviation from the tribimaximal mixing values of the neutrino mixing parameters, namely $\sin\theta_{13} = 0, \sin\theta_{23} = 1/\sqrt{2}, \sin\theta_{12} = 1/\sqrt{3}$ [46,47]. It turns out that, given the recent fit to neutrino oscillation experiments, $r, s, a \sim \mathcal{O}(0.1)$. To simplify the notation, we further introduce $\Delta_{21} = \Delta m^2_{21} L/4E_\nu$, $\Delta_{31} = \Delta m^2_{31} L/4E_\nu$ and $V_{CC} = A_{CC} L/2\Delta_{31} = 2A_{CC}E_\nu/\Delta m^2_{31}$; at the DUNE peak energy, namely 2.5 GeV, we estimate $V_{CC} \sim 0.2$ and we can further expand in the small V_{CC}.

To start with, let us consider the vacuum case; for the $\nu_\mu \to \nu_e$ channel, the leading term of the asymmetry is the following:

$$A^{SM_0}_{\mu e} \;=\; -\frac{12}{f_1}\, r\,\alpha\Delta_{31}\sin\delta\sin^2\Delta_{31}\,, \tag{4}$$

where

$$f_1 \;=\; 9r^2\sin^2\Delta_{31} + 4\alpha\Delta_{31}(\alpha\Delta_{31} + 3r\cos\delta\cos\Delta_{31}\sin\Delta_{31}). \tag{5}$$

Being that the numerator and the denominator of Equation (4) are doubly suppressed by small quantities, we expect $A^{SM_0}_{\mu e} \sim \mathcal{O}(1)$.

For the $\nu_\mu \to \nu_\tau$ channel, on the other hand, we find that the leading contribution to the asymmetry is given by a simpler expression:

$$A^{SM_0}_{\mu\tau} \;=\; \frac{4}{3} r\alpha\Delta_{31}\sin\delta\,, \tag{6}$$

which is clearly smaller than $A_{\mu e}$. Notice also that, differently from $A_{\mu e}$, this asymmetry becomes negative if $\delta > 180^\circ$, as emerging from fits to neutrino oscillation data [2,3].

A third possible asymmetry, namely $A_{\mu\mu}$, is obviously vanishing in vacuum because of CPT conservation, but it can assume a relevant role when matter effects are taken into account (as we will discuss later on).

As it is well known, the inclusion of matter effects complicates the analytic expressions of the transition probabilities and, more importantly, that of the asymmetries. In order to deal with readable formulae, we can work in the regime of weak matter potential $V_{CC} \ll 1$ which, as outlined before, is a good approximation in the case of DUNE. Thus, we can organize our perturbative expansion as follows:

$$A_{\alpha\beta} = A^{SM_0}_{\alpha\beta} + V_{CC}\, A^{SM_1}_{\alpha\beta} + \mathcal{O}(V^2_{CC})\,, \tag{7}$$

where $A^{SM_1}_{\alpha\beta}$ represents the first-order correction to the vacuum case $V_{CC} = 0$. Thus, the asymmetries considered in this study acquire the following corrections:

$$\begin{aligned} A^{SM_1}_{\mu e} \;&=\; -\frac{6}{f_1} r(\Delta_{31}\cos\Delta_{31} - \sin\Delta_{31})\big[2\alpha\Delta_{31}\cos\delta\cos\Delta_{31} + 3r\sin\Delta_{31} + \\ &-\; \frac{24}{f_1} r\alpha^2\sin^2\delta\,\Delta^2_{31}\sin^3\Delta_{31}\Big]\,, \end{aligned} \tag{8}$$

$$A^{SM_1}_{\mu\tau} \;=\; -2r^2(1 - \Delta_{31}\cot\Delta_{31}) + \frac{8}{27}\alpha^2\Delta^3_{31}\cot\Delta_{31}\,, \tag{9}$$

$$A^{SM_1}_{\mu\mu} \;=\; \frac{4}{3} r\alpha\Delta_{31}\cos\delta(\Delta_{31} - \tan\Delta_{31}) - \frac{8}{27}\alpha^2\Delta^3_{31}\tan\Delta_{31}\,. \tag{10}$$

It is evident that $A_{\mu e}$ increases because a term proportional to r^2/f_1 appears, which is of $\mathcal{O}(1)$. Since the r^2/f_1 correction is positive at the atmospheric peak $\sin\Delta_{31} \gg \cos\Delta_{31}$ and adds an $\mathcal{O}(V_{CC})$ contribution to the total $A_{\mu e}$, that at the DUNE peak energy becomes roughly 1/2.

$A_{\mu\tau}^{SM_1}$ contains only terms proportional to $V_{CC}r^2$ and $V_{CC}\alpha^2$ that are not balanced by any small denominator. Thus, both contributions set a correction to the vacuum asymmetry.

A similar situation arises for $A_{\mu\mu}$, where only terms proportional to $V_{CC}r\alpha$ and $V_{CC}\alpha^2$ appear.

3. NSI and CP Asymmetries

As mentioned in the introduction, the uncertainties on the mixing parameters leave room for the possibility of the presence of nonstandard interactions between neutrinos and the particles they meet traveling through the Earth. The strength of such new interactions can be parameterized in terms of the complex couplings $\varepsilon_{\alpha\beta} = |\epsilon_{\alpha\beta}|e^{i\delta_{\alpha\beta}}$, which modify the matter potential of Equation (1) to:

$$A_{CC}\begin{pmatrix} 1+\varepsilon_{ee} & \varepsilon_{e\mu} & \varepsilon_{e\tau} \\ \varepsilon_{e\mu}^* & \varepsilon_{\mu\mu} & \varepsilon_{\mu\tau} \\ \varepsilon_{e\tau}^* & \varepsilon_{\mu\tau}^* & \varepsilon_{\tau\tau} \end{pmatrix}.$$

Since the Hamiltionian has to be Hermitian, the three diagonal couplings $\varepsilon_{\alpha\alpha}$ must be real. Moreover, we can always subtract a matrix proportional to the identity without changing the transition probabilities. If we choose to subtract $\varepsilon_{\mu\mu}\mathbb{I}$, only two independent diagonal parameters ($\varepsilon'_{ee} = \varepsilon_{ee} - \varepsilon_{\mu\mu}$ and $\varepsilon'_{\tau\tau} = \varepsilon_{\tau\tau} - \varepsilon_{\mu\mu}$) will appear in the NSI matrix. Notice that, since from non-oscillation experiments bounds on $\varepsilon_{\mu\mu}$ are very stringent, $\varepsilon'_{ee} \sim \varepsilon_{ee}$ and $\varepsilon'_{\tau\tau} \sim \varepsilon_{\tau\tau}$. Thus, beside the standard oscillation angles and phases, the parameter space is enriched by five more moduli $|\varepsilon_{\alpha\beta}|$ and three more phases $\phi_{\alpha\beta}$, which could provide new sources of CP violation in the lepton sector.

Asymmetries in the NSI Framework

Since NSI effects are strongly intertwined with standard matter effects driven by V_{CC}, the asymmetries can be cast in a form which generalizes Equation (7):

$$A_{\alpha\beta} = A_{\alpha\beta}^{SM_0} + V_{CC}(A_{\alpha\beta}^{SM_1} + A_{\alpha\beta}^{NSI}) + \mathcal{O}(V_{CC}^2)\,, \tag{11}$$

where $A_{\alpha\beta}^{SM_{0,1}}$ refers to the pure Standard Model results and all the effects of the NSI are included in the $A_{\alpha\beta}^{NSI}$ term.

Bounds on the magnitude of the NSI couplings have been widely discussed [34]; even though some of them could, in principle, be of $\mathcal{O}(1)$ and give rise, for example, to degeneracies leading to the so-called LMA-Dark solution [48], we decided nonetheless to consider all $\varepsilon_{\alpha\beta}$'s on the same footing and of the same order of magnitude as the other small standard parameters a, s, r, α and V_{CC}. In this way, we are able to catch the leading dependence on NP carried on by the CP asymmetries.

For the $\nu_\mu \to \nu_e$ channel, the leading order NSI contributions can be arranged as follows:

$$A_{\mu e}^{NSI} = \varepsilon_{e\mu}a_{\mu e}^{\varepsilon_{e\mu}} + \varepsilon_{e\tau}a_{\mu e}^{\varepsilon_{e\tau}}\,, \tag{12}$$

where the $a's$ functions are given by:

$$\begin{aligned} a_{\mu e}^{\varepsilon_{e\mu}} &= \frac{3}{f_1}\big[6r\cos(\delta-\delta_{e\mu})\sin\Delta_{31}(\Delta_{31}\cos\Delta_{31}+\sin\Delta_{31}) + \\ &\quad 4\alpha\Delta_{31}\cos\delta_{e\mu}(\Delta_{31}+\cos\Delta_{31}\sin\Delta_{31})\big] \\ &- \frac{72}{f_1^2}r\alpha\sin\delta\Delta_{31}^2\sin^4\Delta_{31}\big[3r\sin(\delta-\delta_{e\mu})+2\alpha\sin\delta_{e\mu})\big]\,, \end{aligned} \tag{13}$$

$$
\begin{aligned}
a_{\mu e}^{\varepsilon_{e\tau}} &= \frac{3}{f_1}[6r\cos(\delta-\delta_{e\tau})\sin\Delta_{31}(-\Delta_{31}\cos\Delta_{31}+\sin\Delta_{31}) + \\
&\quad 2\alpha\Delta_{31}\cos\delta_{e\tau}(-2\Delta_{31}+\sin 2\Delta_{31})] \\
&+ \frac{72}{f_1^2} r\alpha\sin\delta\Delta_{31}^2\sin^4\Delta_{31}[3r\sin(\delta-\delta_{e\tau})-2\alpha\sin\delta_{e\tau}]\,.
\end{aligned} \tag{14}
$$

For the sake of simplicity, the symbols $\varepsilon_{\alpha\beta}$ with $\alpha \neq \beta$ indicate the moduli of such parameters. The only NP parameters appearing at the considered perturbative level are $\varepsilon_{e\mu}$ and $\varepsilon_{e\tau}$ which, in turn, carry the dependence on the CP phases $\delta_{e\mu}, \delta_{e\tau}$. All in all, the NSI contributions set an $\mathcal{O}(V_{CC})$ correction to $A_{\mu e}^{SM_0}$. We also notice that the largest of the considered terms, namely the ones linear in r in the numerator, have similar expressions in both $a_{\mu e}^{\varepsilon_{e\mu}}$ and in $a_{\mu e}^{\varepsilon_{e\tau}}$, apart from the sign in front of $\cos\Delta_{31}$. This means that, around the atmospheric peak, the phases $\delta_{e\mu}$ and $\delta_{e\tau}$ are equally important, even though the magnitude of their impact strongly depends on the value of the standard CP phase δ.

For the asymmetry in the $\mu\tau$-channel, we found the following structure:

$$
\begin{aligned}
A_{\mu\tau}^{NSI} &= 8\varepsilon_{\mu\tau}\cos\delta_{\mu\tau}\Delta_{31}\cot\Delta_{31} + \\
&- \frac{4}{3}\alpha\Delta_{31}^2\left(\varepsilon_{e\mu}\cos\delta_{e\mu}-\varepsilon_{e\tau}\cos\delta_{e\tau}-4\varepsilon_{\mu\tau}\cos\delta_{\mu\tau}\csc^2\Delta_{31}\right) + \\
&- 2r\left[\varepsilon_{e\mu}\cos(\delta-\delta_{e\mu})+\varepsilon_{e\tau}\cos(\delta-\delta_{e\tau})\right](1-\Delta_{31}\cot\Delta_{31}) \\
&+ 4a\varepsilon'_{\tau\tau}(1-\Delta_{31}\cot\Delta_{31})\,.
\end{aligned} \tag{15}
$$

In this case, four different NSI parameters enter the leading order corrections, namely $\varepsilon_{\mu\tau}, \varepsilon_{e\tau}, \varepsilon_{e\mu}$ (together with their phases) and $\varepsilon'_{\tau\tau}$. Contrary to the μe case, the largest correction to the vacuum expression is given by the first-order term $\varepsilon_{\mu\tau}$ in the first line of Equation (15), which is not suppressed by any of the standard small parameters a, r, s and α. Considering that $A_{\mu\tau}^{SM_0} \sim \mathcal{O}(r\alpha)$, this makes the $\mu\tau$-channel promising for searching for NP, at least at the probability level where possible complications due to small τ statistics do not enter.

Finally, for the $\mu\mu$ channel, matter effects generate a substantial difference in the propagation of neutrinos versus antineutrinos, which results in the following NSI contributions:

$$
\begin{aligned}
A_{\mu\mu}^{NSI} &= -8\varepsilon_{\mu\tau}\Delta_{31}\cos\delta_{\mu\tau}\tan\Delta_{31} - 4r\varepsilon_{e\mu}\Delta_{31}\cos\left(\delta-\delta_{e\mu}\right)\tan\Delta_{31} + \\
&+ 4a\varepsilon'_{\tau\tau}(\Delta_{31}-\tan\Delta_{31})\tan\Delta_{31} - \frac{4}{3}\alpha\Delta_{31}\times \\
&\quad \left[\varepsilon_{e\mu}\cos\delta_{e\mu}(\Delta_{31}+\tan\Delta_{31}) - \varepsilon_{e\tau}\cos\delta_{e\tau}(\Delta_{31}-\tan\Delta_{31}) - \right. \\
&\quad \left. 4\Delta_{31}\varepsilon_{\mu\tau}\cos\delta_{\mu\tau}\sec^2\Delta_{31}\right]\,.
\end{aligned} \tag{16}
$$

As expected from unitarity relations, we get an opposite linear dependence on $\varepsilon_{\mu\tau}$ but with a coefficient proportional to $\tan\Delta_{31}$ which, close to the atmospheric peak, gives an important correction to $A_{\mu\mu}^{SM_1}$.

4. Sterile Neutrinos and CP Asymmetries

The next NP scenario under discussion is the so-called $3+1$ model, in which a sterile neutrino state supplements the three standard active neutrinos. Even though the new state cannot interact with the ordinary matter, it can have a role in neutrino oscillations thanks to the mixing with the active partners. The longstanding reactor, gallium, and short-baseline anomalies [21] suggested that, if present, the fourth mass eigenstate m_4 should have a mass, such that $\Delta m_{41}^2 = m_4^2 - m_1^2 \sim \mathcal{O}(1)\ \mathrm{eV}^2$, that is orders of magnitude larger than the solar and the atmospheric mass splittings, and that is thus capable of driving fast oscillations visible at accordingly small L/E. In addition to the new mass splitting Δm_{41}^2, the PMNS matrix becomes a 4×4 matrix that can be parametrized in terms of 6 angles and 3 phases.

In this manuscript, we adopt the following multiplication order of the rotation matrices $R(\theta_{ij})$ [49–51]:

$$U = R(\theta_{34})R(\theta_{24})R(\theta_{23},\delta_3)R(\theta_{14})R(\theta_{13},\delta_2)R(\theta_{12},\delta_1). \tag{17}$$

Apart from δ_2, which becomes the standard CP phase for $m_4 \to 0$, we have two potential new sources of CP violation, encoded in two phases δ_1 and δ_3. In the description of neutrino propagation in matter, we cannot disregard the role of the NC interactions because the sterile state does not feel at all the presence of matter; this results in the following evolution equations:

$$i\frac{d}{dt}\begin{pmatrix} \nu_e \\ \nu_\mu \\ \nu_\tau \\ \nu_s \end{pmatrix} = \tag{18}$$

$$= \left[\frac{1}{2E_\nu}U\begin{pmatrix} 0 & 0 & 0 & 0 \\ 0 & \Delta m^2_{21} & 0 & 0 \\ 0 & 0 & \Delta m^2_{31} & 0 \\ 0 & 0 & 0 & \Delta m^2_{41} \end{pmatrix}U^\dagger + \begin{pmatrix} A_{CC}+A_{NC} & 0 & 0 & 0 \\ 0 & A_{NC} & 0 & 0 \\ 0 & 0 & A_{NC} & 0 \\ 0 & 0 & 0 & 0 \end{pmatrix}\right]\begin{pmatrix} \nu_e \\ \nu_\mu \\ \nu_\tau \\ \nu_s \end{pmatrix},$$

where ν_s is the new sterile state, A_{CC} is the usual matter charged current potential, and A_{NC} is the matter NC potential, $A_{NC} \equiv 1/\sqrt{2}G_F n_n$, with n_n being the neutron density in the Earth crust.

Asymmetries in $3+1$ *Framework*

The parameter space of the $3+1$ model is enlarged compared to the SM case by three new mixing angles θ_{i4}, two more CP phases $\delta_{1,3}$, and the mass-squared difference Δm^2_{41}. Thus, in addition to the expansion parameters used in the previous sections (r, s, a), we also expand in the small s_{14}, s_{24} and s_{34} (where $s_{i4} = \sin\theta_{i4}$) that we can still assume of $\mathcal{O}(0.1)$. To further simplify the analytic expressions of the asymmetries, we also introduce $V_{NC} = A_{NC}L/2\Delta_{31}$. It is useful to present the results in a form similar to Equation (11):

$$A_{\alpha\beta} = A^{SM}_{\alpha\beta} + A^{3+1}_{\alpha\beta} + \mathcal{O}(\lambda^n)\,, \tag{19}$$

where $A^{SM}_{\alpha\beta}$ are the SM asymmetries and the symbol λ represents a common order of magnitude of all small quantities used in our perturbation theory, including V_{CC} (but not V_{NC}, whose dependence in $A_{\alpha\beta}$ is exact). The exponent amount to $n = 3$ for $A_{\mu\tau}, A_{\mu\mu}$ and $n = 2$ for $A_{\mu e}$. Notice that the SM phase δ of Equations (4)–(10) must be replaced by the combination $\delta_2 - \delta_1 - \delta_3$ due to the parametrization adopted in this manuscript. Averaging out all of the fast oscillations driven by Δm^2_{41}, the various $A^{3+1}_{\alpha\beta}$ have the following expressions:

$$\begin{aligned} A^{3+1}_{\mu e} &\sim \frac{s_{14}s_{24}}{f_1}\{-6[2\alpha\Delta_{31}\sin\delta_1 + 3r\cos\Delta_{31}\sin(\delta_2-\delta_3)\sin\Delta_{31}]\} + \\ &\quad \frac{s_{14}s_{24}}{f_1^2}\{216r^2\alpha\Delta_{31}\cos(\delta_2-\delta_3)\sin(\delta_1-\delta_2+\delta_3)\,\sin^4\Delta_{31}\}\,, \\ A^{3+1}_{\mu\tau} &= 2s_{24}s_{34}\cot\Delta_{31}(\sin\delta_3 - 2V_{NC}\Delta_{31}\cos\delta_3)\,, \\ A^{3+1}_{\mu\mu} &= 4s_{24}s_{34}V_{NC}\Delta_{31}\cos\delta_3\tan\Delta_{31}\,. \end{aligned} \tag{20}$$

To avoid large expressions, for $A_{\mu e}$, we only quote the corrections due to the new mixing angles.

First of all, we notice that the corrections to the μe asymmetry are only linearly suppressed compared to the leading order results; thus, we expect such an asymmetry to be quite sensitive to new sources of CP violation. Then, both corrections to the $\mu\tau$ and the $\mu\mu$ asymmetries are linear in the combination $s_{24}s_{34}$. Since the angle θ_{34} has weak

constraints (values of 20–30° are still allowed), these corrections can be relatively large. Notice also that $A^{3+1}_{\mu\tau}$ is expected to provide a large correction to the standard model asymmetries since V_{NC} is roughly of the same order of magnitude as V_{CC}; this makes the ν_τ appearance channel, at least in principle, sensitive to NP effects. As for the PMNS phases, all leading order corrections depend only on the new phase δ_3. This means that a long baseline experiment is mostly sensitive only to the combination $\delta_2 - \delta_1 - \delta_3$ and to the single phase δ_3.

Beside the results of Equation (20), it is worth considering a new asymmetry corresponding to the $\nu_\mu \to \nu_s$ transition. Even though sterile neutrinos cannot be directly detected, the probability $P(\nu_\mu \to \nu_s)$ is a measure of the NC events in the detector. Indeed, given that the NC interactions flavor independent, the number of events is proportional to the sum of the transition probabilities from the starting flavor (ν_μ) to the three active final flavors ($\nu_{e,\tau,\mu}$) because of the unitarity relation $P(\nu_\mu \to \nu_s) = 1 - P(\nu_\mu \to \nu_{e,\mu,\tau})$. The new asymmetry has vanishing matter corrections and, at the leading nonvanishing order, reads:

$$A^{3+1}_{\mu s} = -\frac{2 s_{24} s_{34} \sin\delta_3 \sin\Delta_{31} \cos\Delta_{31}}{2 s_{24}^2 + (s_{34}^2 - s_{24}^2)\sin^2\Delta_{31}} \,. \tag{21}$$

This is clearly an $\mathcal{O}(1)$ result since both numerator and denominator are of $\mathcal{O}(\lambda^2)$. In Table 1, we summarize the outcome of our analytic considerations on the magnitude of the NP corrections to the asymmetries discussed in this paper.

Table 1. Order of magnitude estimates of the various contributions to the asymmetries discussed in this paper. λ is a common order parameter such that: $r, s, a, \Delta_{21}, V_{CC}, \varepsilon_{\alpha\beta}, \theta_{i4} \sim \mathcal{O}(\lambda)$.

Asymmetry	SM	NSI	3+1
$A_{\mu e}$	1	λ^2	λ
$A_{\mu\mu}$	λ^3	λ^2	λ^2
$A_{\mu\tau}$	λ^2	λ^2	λ^2
$A_{\mu s}$	-	-	1

5. The DUNE Experiment

The DUNE (Deep Underground Neutrino Experiment) experiment is a proposed long-baseline experiment based in the USA [41–44]. The accelerator facility and the near detector will be located at Fermilab, while a 40 kt far detector is going to be built at the SURF (Sanford Underground Research Facility) laboratories in South Dakota, 1300 km away from the neutrino source.

Both far and near detectors will be LAr-TPCs, namely detectors with good imaging capabilities, which are expected to collect a huge number of different neutrino interaction events.

The neutrino beam, produced after proton interactions on a 95-cm-long cylindrical graphite target, will be a ν_μ beam (roughly 10^{10} ν-s/m^2/GeV/10^{20} POT at the peak energy at 1300 km from the source) with a small ν_e contamination (10^7 ν-s/m^2/GeV/10^{20} POT). Focusing horns, which are able to select particles with a given electric charge before the decay tunnel, will produce particle and antiparticles beams, allowing the experiment to run in two different modes, namely the ν-mode and the $\bar{\nu}$-mode. The neutrino flux energy spectra should be peaked at $E_{peak} = 2.5$ GeV; however, different proposals have been promoted for higher energy fluxes (see [52–54] for a discussion on NP sensitivities of DUNE with neutrino beams spanning a wide range of energies). Indeed, even though E_{peak} is the energy of the atmospheric peak of the oscillation probabilities at 1300 km baseline, we are below the τ production threshold ($E_{thr} = 3.1$ GeV). Thus, with such a flux, CC interactions of the huge number of ν_τ-s arriving at the far detector are forbidden. A broader and more energetic flux would overcome this problem, allowing the τ neutrinos to be energetic enough to produce τ leptons. This τ-optimized flux [55,56] would be less useful in constraining oscillation parameters from ν_e appearance channel (due to the increased

number of background events such as misidentified ν_τ-s) but, at the same time, very useful for NP searches thanks to the increased number of ν_τ events.

In order to simulate the DUNE experiment, we used the GLoBES package [57,58]. Initial fluxes, far detector efficiencies and energy resolutions, exposure time (which has been chosen as 3.5 years in ν-mode and 3.5 years in $\bar{\nu}$-mode), beam power (14.7×10^{20} POT/year) backgrounds, and systematic uncertainties have been provided by the DUNE collaboration for the ν_e appearance and ν_μ disappearance channels [59,60]. For the former, backgrounds are misidentified ν_μ, ν_τ, and NC events, as well as ν_e-s from the flux contamination; for the latter, the main background source are NC events. Systematic normalization uncertainties at the far detector are 2% for the ν_e appearance signal and 5% for the ν_μ disappearance signal, numbers proposed by the DUNE collaboration from the foreseen performance of the near detector.

In the last several years, the possibility to study also the ν_τ appearance and the NC channels as signals have been taken into account. For the first one, the use of the hadronic and electronic decays of τ leptons to identify the event topology have been discussed in [61,62]. According to the cited literature, we used an efficiency of 30% for both electronic and hadronic decay events, 20% systematic normalization uncertainty, and misidentified ν_e and NC events as backgrounds. For the NC channel, 90% effieciency, 10% systematic uncertainty, and 10% of the ν_μ events as a background have been proposed in [63] and adopted here.

Effects of NSI and Sterile Neutrinos on DUNE Spectra

Before discussing the sensitivity on the CP asymmetries, it is useful to have a look at the effects of new physics on the neutrino spectra, which will help in the interpretation of our numerical results.

For the NSI case, different global analyses on oscillation experiments have been conducted [30,33,34]. The 2σ current limits on the various $\varepsilon_{\alpha\beta}$ from [30] have been summarized in Table 2.

Table 2. 2σ bounds on the moduli of the NSI parameters, from [30].

NSI Parameters	2σ Bounds
ε'_{ee}	$(-0.2\ ,\ 0.45)$
$\varepsilon'_{\tau\tau}$	$(-0.02\ ,\ 0.175)$
$\lvert\varepsilon_{e\mu}\rvert$	<0.1
$\lvert\varepsilon_{e\tau}\rvert$	<0.3
$\lvert\varepsilon_{\mu\tau}\rvert$	<0.03

Scanning the NSI parameters in the allowed ranges and taking the new phases $\delta_{e\mu}$, $\delta_{e\tau}$, and $\delta_{\mu\tau}$ in the range $[0, 2\pi]$ (both sets of parameters extracted randomly flat), we get the neutrino and antineutrino spectra at the far detector, as shown in Figure 1. The number of events is normalized by the bin width and the exposure for both ν-mode and $\bar{\nu}$-mode is 3.5 years.

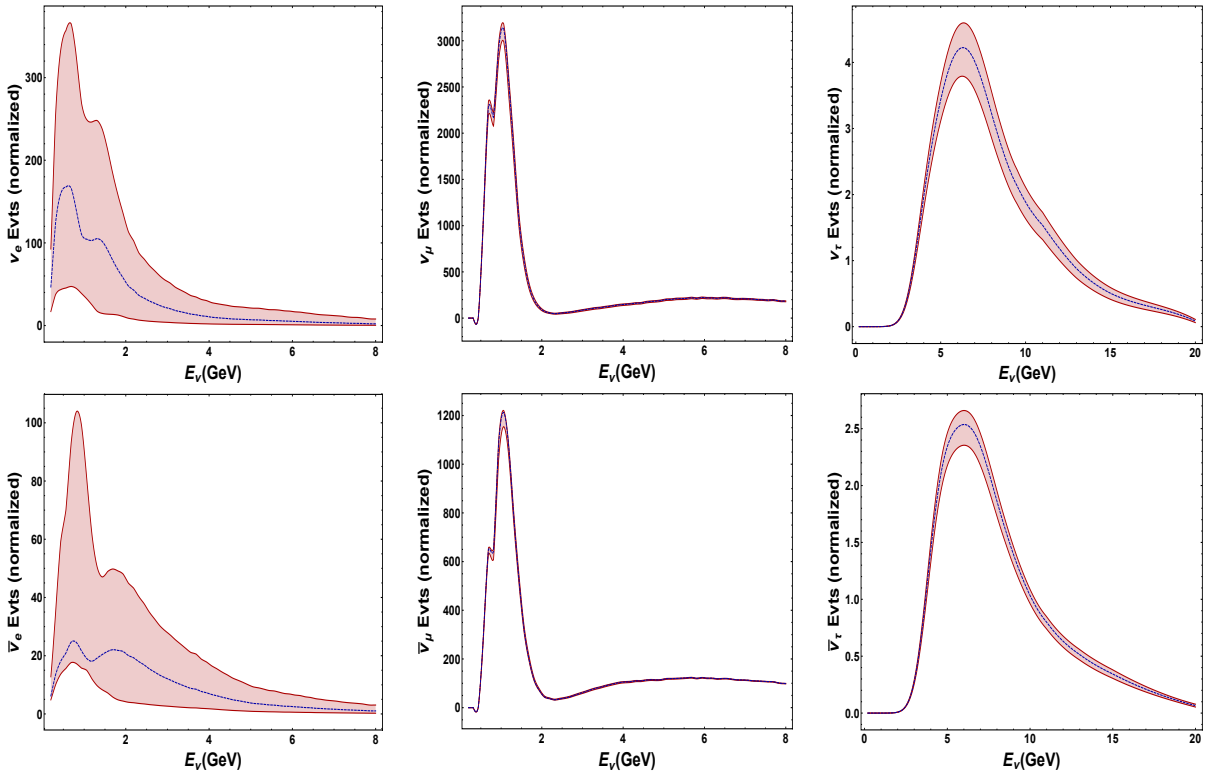

Figure 1. Expected number of neutrino (upper panels) and antineutrino (lower panels) events at the DUNE far detector as a function of the neutrino energy. The (orange) bands show the effects of including the NSI parameters in the transition probabilities; the blue dashed line refers to the spectra obtained in the standard model. The best fits for the standard oscillation angles and phase and mass differences are taken from [2] and reported in Table 3. Standard fluxes for neutrinos have been used.

In all panels, the blue dashed lines refer to the spectra obtained in the standard oscillation framework with normal hierarchy (NH), for which the best fit values are summarized in Table 3.

Table 3. Best fits for oscillation parameters obtained by the global analysis in [2].

Oscillation Parameters	Best Fits (NH)	Best Fits (IH)
$\theta_{12}/^\circ$	$33.44^{+0.78}_{-0.75}$	$33.45^{+0.78}_{-0.75}$
$\theta_{13}/^\circ$	$8.57^{+0.13}_{-0.12}$	$8.61^{+0.12}_{-0.12}$
$\theta_{23}/^\circ$	$49^{+1.1}_{-1.4}$	$49.3^{+1.0}_{-1.3}$
$\delta/^\circ$	195^{+51}_{-25}	286^{+27}_{-32}
$\frac{\Delta m^2_{21}}{10^{-5}\ eV^2}$	$7.42^{+0.21}_{-0.20}$	$7.42^{+0.21}_{-0.20}$
$\frac{\Delta m^2_{31}}{10^{-3}\ eV^2}$	$2.514^{+0.028}_{-0.027}$	$-2.497^{+0.028}_{-0.028}$

The figures clearly show that the ν_e and $\bar{\nu}_e$ spectra are the ones affected the most by the NSI parameters. This is because at the DUNE energies and baseline, the SM ν_e appearance probability is suppressed and the resulting effects of the NSI parameters are more evident—in particular, the resulting effect of $\varepsilon_{e\tau}$, which has weaker bounds compared to the others. Conversely, in the ν_μ spectra, the NSI have a very small impact. In fact, in the disappearance probability, the first term is of $\mathcal{O}(1)$, and the largest NSI corrections is driven by $\varepsilon_{\mu\tau}$, which has strong bounds $\sim \mathcal{O}(10^{-3})$.

Finally, in the ν_τ appearance channel, the modifications in the spectra due to the NSI are evident, but, due to the small number of expected events, the changes with respect to the SM case are difficult to observe.

If we repeat the same study using the high-energy τ-optimized flux we get similar features as before, but for the ν_τ events, which are obviously much larger (see Figure 2; notice that wiggles near the disappearance spectra peaks are an artifact of extrapolating the smearing matrices from $\mathcal{O}(1)$ GeV to high energies).

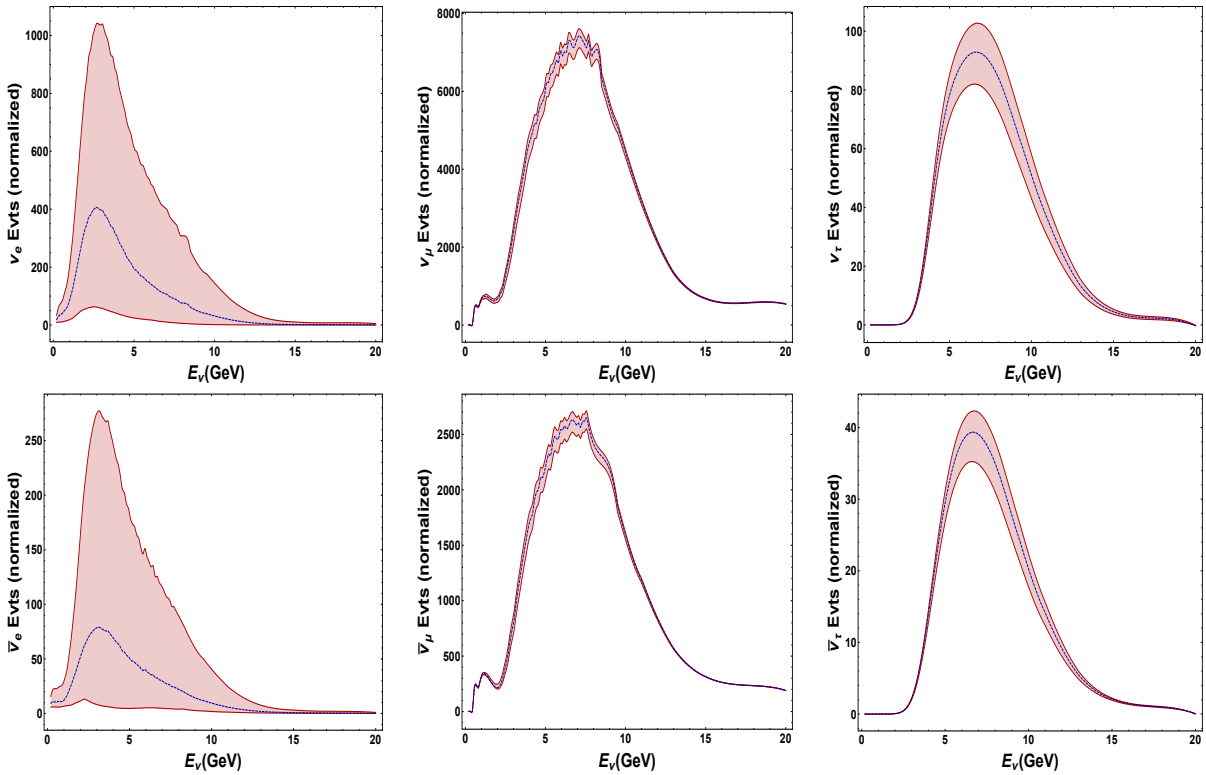

Figure 2. Same as Figure 1 but using the τ-optimized flux.

In the $3+1$ framework, bounds on the parameters strongly depend on the adopted parametrization of the 4×4 mixing matrix U. In addition, transition probabilities are affected by many degeneracies among standard and nonstandard mixing angles that makes the extraction of the allowed/excluded ranges more complicated. However, in the parametrization of Equation (17), if we allow the standard parameters to vary only in their allowed ranges (Table 3) and we fix the new mass splitting to be $\Delta m^2_{41} \sim 1$ eV^2, different studies [21,22] suggest that θ_{14} and θ_{24} can be taken in the range $[0\text{–}10]^\circ$ while θ_{34} in the range $[0\text{–}30]^\circ$. The variations of the neutrino spectra for the $3+1$ model are shown in Figures 3 and 4.

As for the NSI case, the largest deviation from the SM results are found in the ν_e spectra, since, as showed in Equation (20), the $3+1$ corrections to the standard asymmetry are at the first order of our expansion.

As for the other flavors, the ν_μ spectra are not really affected by NP, while the deviation of the ν_τ spectra from the SM predictions can be mostly ascribed to θ_{34} and its relatively large allowed range. We also see that the contributions to NSI are mainly negative, as it should be because the corrections to the probabilities driven by θ_{34} are negative indeed.

Computing the same spectra using the τ-optimized flux (Figure 4), the changes in the ν_τ appearance channel, as in the NSI case, are amplified.

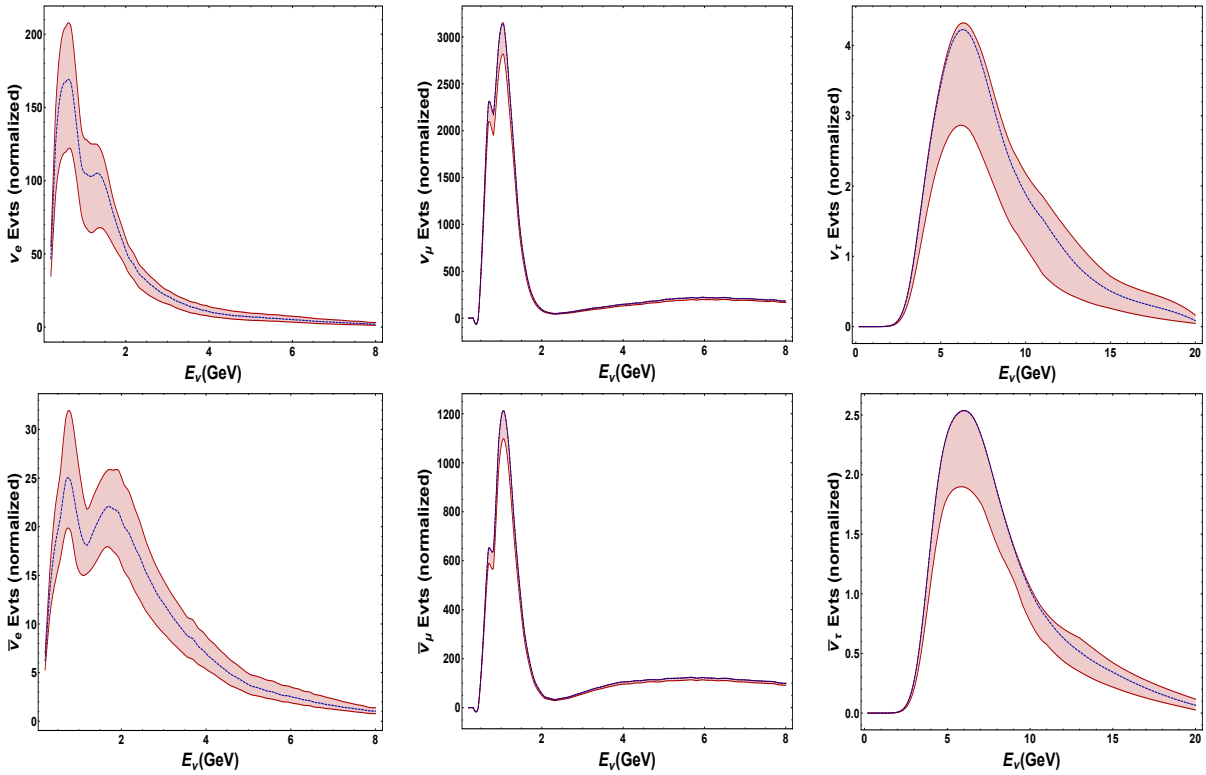

Figure 3. Same as Figure 1 but for the $3+1$ neutrino mass model.

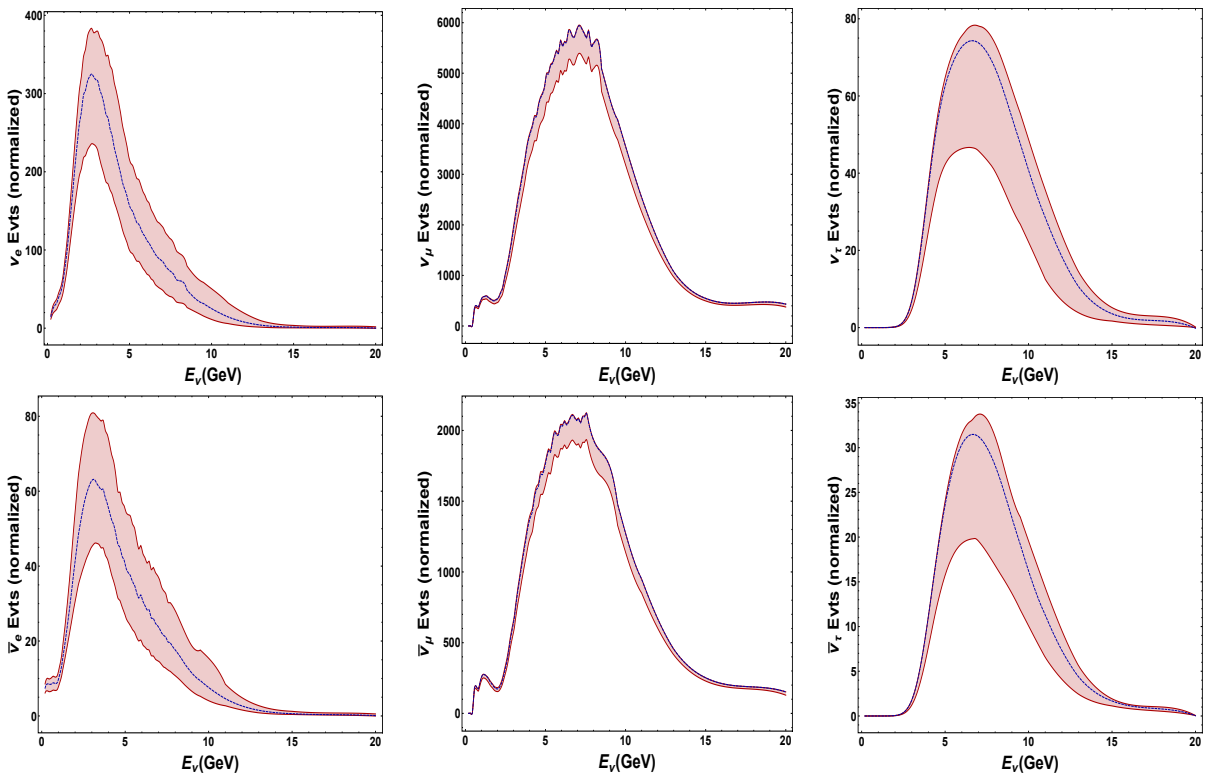

Figure 4. Same as Figure 2 but for the $3+1$ neutrino mass model.

6. Numerical Evaluation of Asymmetries

The relevant question now is related to the experimental capability to measure the asymmetries we are considering: in fact, if the CP violating quantities will not be measured

with a sufficient precision, then we cannot distinguish the deviation from the SM results due to NP. Instead of considering the asymmetries at the probability level, we deal with the experimentally relevant integrated asymmetries built from the number of expected events N_β and $\bar{N}_\beta$:

$$A_{\alpha\beta} = \frac{N_\beta - \bar{N}_\beta}{N_\beta + \bar{N}_\beta}, \tag{22}$$

where the event rates for the $\nu_\alpha \to \nu_\beta$ and the CP conjugate $\bar{\nu}_\alpha \to \bar{\nu}_\beta$ transitions are computed from:

$$N_\beta = \int_{E_\nu} dE_\nu \, P_{\alpha\beta}(E_\nu) \, \sigma_\beta(E_\nu) \, \frac{d\phi_\alpha}{dE_\nu}(E_\nu) \, \varepsilon_\beta(E_\nu) \tag{23}$$

$$\bar{N}_\beta = \int_{E_\nu} dE_\nu \, P_{\bar{\alpha}\bar{\beta}}(E_\nu) \, \sigma_{\bar{\beta}}(E_\nu) \, \frac{d\phi_{\bar{\alpha}}}{dE_\nu}(E_\nu) \, \varepsilon_\beta(E_\nu), \tag{24}$$

in which $\sigma_{\beta(\bar{\beta})}$ is the cross-section for producing the lepton $\beta(\bar{\beta})$ (we used NC and CC inclusive cross sections from GENIE 2.8.4 included in the DUNE GLoBES files [59], which are of the order of $\sigma/E = 10^{-39}$–10^{-38} cm^2/GeV), and $\varepsilon_{\beta(\bar{\beta})}$ is the detector efficiency to reveal that lepton and $\phi_{\alpha(\bar{\alpha})}$ the initial neutrino flux at the source. Since in the SM, the only dependence on the CP phase is carried on by δ, the correlations between the pair of asymmetries—for instance, $(A_{\mu\tau}, A_{\mu e})$ and $(A_{\mu\tau}, A_{\mu\mu})$—is maximal and a close curve appears in the related physical planes. If, in addition, we also take the experimental errors on angles and mass differences into account, the curves are scattered as reported in Figure 5 for the DUNE standard flux and in Figure 6 for the optimized flux. The blue dots are obtained using parameters in the normal hierarchy; the orange ones are obtained using the inverse hierarchy hypothesis.

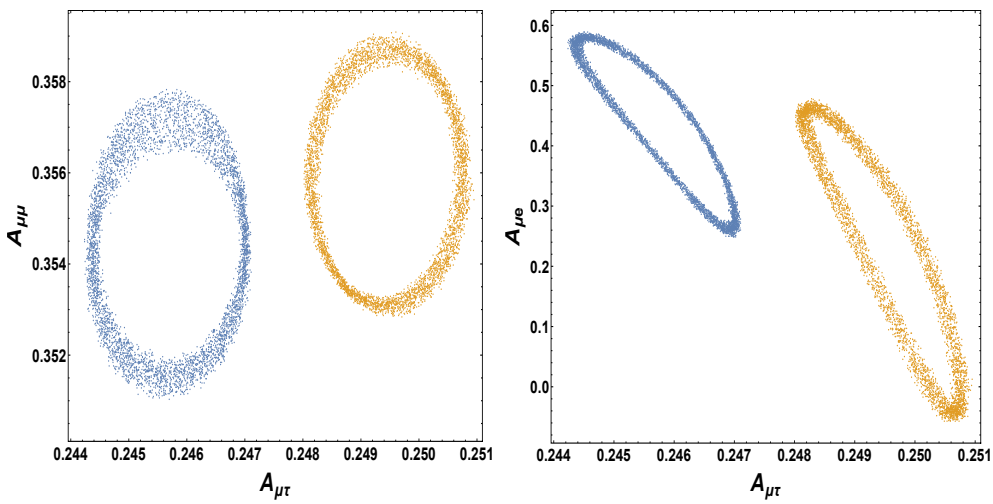

Figure 5. Numerical evaluation of the SM asymmetries of Equation (22) at DUNE, with standard flux. The SM parameters have been allowed to vary in their 1σ range, while all possible values for the CP phase have been taken into account. The blue dots represent asymmetries in the normal hierarchy hypothesis; the orange ones represent asymmetries in the inverted hierarchy hypothesis.

The first striking features of the integrated asymmetries is related to the fact that their sign is always positive; in fact, being integrated quantities, they are influences not only by the relative differences among ν and $\bar{\nu}$ probabilities but also by the differences among ν and $\bar{\nu}$ fluxes and cross sections. As we can observe in Figure 1, the SM spectra (blue lines) of $\bar{\nu}$ is always lower, and this helps in justifying the observed signs. The other important observation is that, as discussed above, $A_{\mu e}$ is the asymmetry that changes the most with

a change of the CP phase. On the other hand, the other two asymmetries $A_{\mu\tau}$ and $A_{\mu\mu}$ change at a much slower rate.

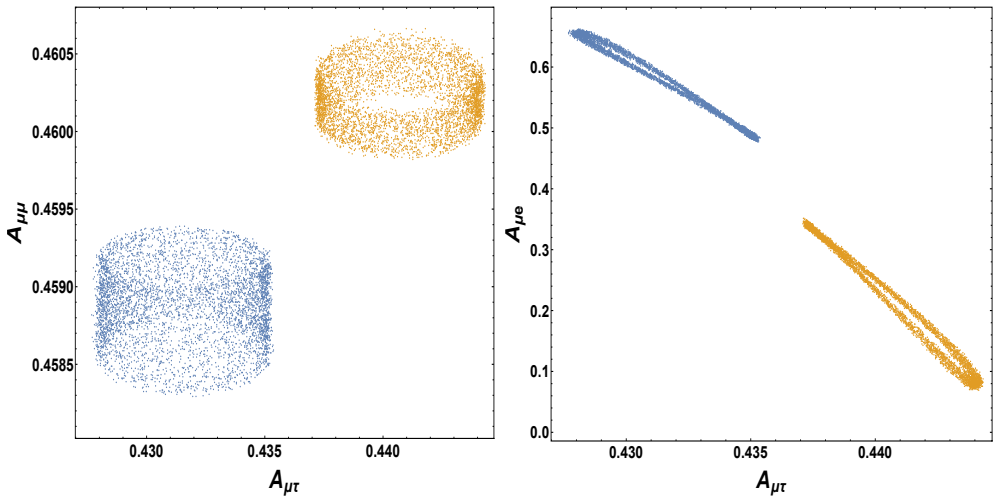

Figure 6. Same as Figure 5 but with the optimized flux. Notice the different vertical scales on the left and right panels.

Eventually, it is worth mentioning that, for each pair of asymmetries, the closed curves corresponding to NH and IH never overlap. This means that, at least in principle, one could be able to solve the neutrino hierarchy problem simply looking at the CP asymmetries. However, in DUNE as well as in other future experiments, the foreseen experimental errors on such asymmetries will probably be too large to allow for such a discrimination, as we will discuss later on in the manuscript.

6.1. Numerical Evaluation of the Asymmetries in Presence of NSI

Now, we are ready to apply our strategy to check whether other sources of CP violation carried on by NP can be sufficiently distinguished from the SM phase. In order to do that, we first need to evaluate the experimental errors on the SM asymmetries and then recompute them as predicted by the NSI and the $3+1$ sterile models. From Figure 5 we see that the uncertainties on the standard angles and mass splittings are not playing an important role. A simple but accurate estimate from error propagation gives:

$$(\delta A_{\alpha\beta})^2 = \frac{4\bar{N}_\beta^2(\delta N_\beta)^2 + 4N_\beta^2(\delta\bar{N}_\beta)^2}{(N_\beta + \bar{N}_\beta)^4}\,, \tag{25}$$

where δN is the uncertainty related to the number of expected events, which receives contributions from the systematic error (normalization errors cited in Section 5) and the statistical error. For the ν_μ disappearance channel, the first source of uncertainty is always dominating, since the number of events is large and the statistical error is reduced. On the other hand, in the other two channels, both terms are important. In particular, in the ν_τ appearance, systematic errors are quite large (due to the poorly known cross-section and to the systematics related to the complicated event reconstruction) and the number of events is small. Thus, we expect $\delta A_{\mu\tau}$ to be particularly large.

In Figure 7, we show the values of the asymmetries where the effects of NSI are taken into account, computed by using the standard neutrino flux. The blue stars represent the asymmetries in the standard case fixing all the standard parameters to their best fits but varying the values of δ (we present here only results in the normal hierarchy; for the inverted hierarchy case, the conclusions are very similar); the orange dots are the results obtained in presence of NSI, computed from the number of events corresponding to random flat extraction of the couplings in the ranges shown in Table 2. The sides of the grey rectangles represent the maximum 1σ error bars on the standard asymmetries at different chosen values of δ as computed from

Equation (25). For the sake of illustration, we do not show the error bars associated to the NSI points here because the number of events is not very different from the standard case, thus the error bars in the NSI framework are of the same order of magnitude as the displayed ones.

It is clear that $A_{\mu\tau}$ is sensitive to new physics. Indeed, the SM asymmetry has almost a fixed value $A_{\mu\tau} \sim 0.245$, as shown in Figure 5, while the NSI contributions can turn $A_{\mu\tau}$ into the range [0.21, 0.27]. However, the error bars are much larger than the produced variation, making this asymmetry at the DUNE conditions not useful for discerning new CP phases. Even though the $A_{\mu e}$ asymmetry gets different values in the standard case (in the range [0.28, 0.55]), the inclusion of the NSI is able to even extend the foreseen asymmetry beyond such a range, enough to reach values outside the error bars of the standard asymmetries. The problem in this case is that, as discussed before, we should also take the error bars on the orange dots into accountso that, when we include them, also $A_{\mu e}$ cannot give hints of NP at DUNE. Finally, for $A_{\mu\mu}$, the same analysis conducted for $A_{\mu\tau}$ applies.

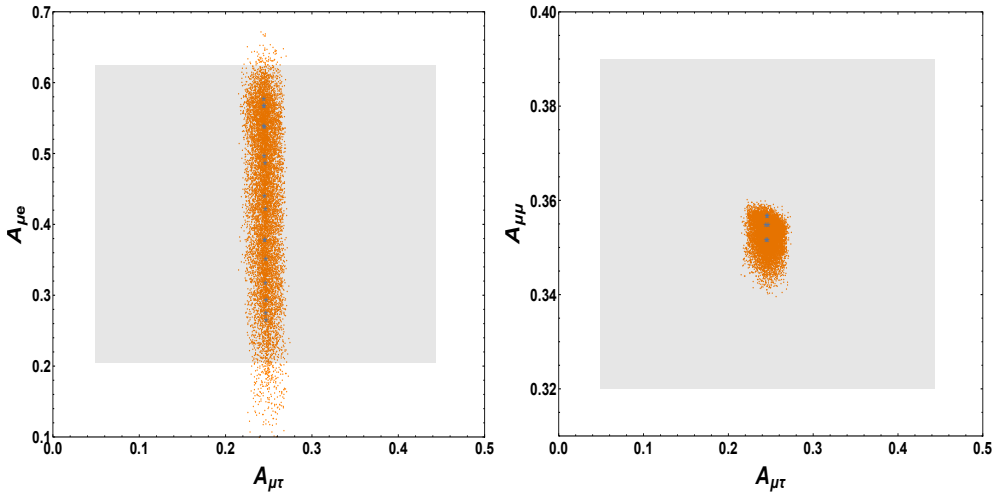

Figure 7. Integrated asymmetries in the $(A_{\mu\tau}, A_{\mu e})$ (**left** plot) and $(A_{\mu\tau}, A_{\mu\mu})$ planes (**right** plot). Blue stars represent the asymmetries in the SM case; the orange dots are the values obtained in the presence of NSI. The grey rectangle shows the 1σ error range on the standard asymmetries. For sake of simplicity, we do not report the error bars on the orange dots here. Standard neutrino flux has been employed to compute the number of events.

With a higher energy flux, the results partially differ from what illustrated above (see Figure 8). Even though the larger number of events reduces the error bars, the $A_{\mu\tau}$ and $A_{\mu\mu}$ with NSI do not change enough in such a way to be clearly distinguished at an acceptable confidence level from the SM case. $A_{\mu e}$ can assume values different from the SM ones; in particular, a sets of NSI parameters can push it toward negative values. Indeed, as it is clear from Equations (12)–(14), NSI corrections to the asymmetries can be comparable to the SM case when $\varepsilon_{e\mu}$ and $\varepsilon_{e\tau}$ are of $\mathcal{O}(0.1)$. With higher energy fluxes, the appearance transition probabilities are mainly evaluated off peak, making the cosine of Δ_{31} in Equations (13) and (14) no longer negligible. Thus NSI corrections become more and more important, causing an opposite sign of the asymmetry with respect to the SM case when $\cos(\delta - \delta_{e\mu,\tau})$ terms become negative.

6.2. Numerical Evaluation of the Asymmetries in the $3+1$ *Sterile Neutrino Model*

In Figure 9, we report our numerical results for the $3+1$ case, obtained for fixed $\Delta m^2_{41} = 1$ eV^2 and all mixing angles and phases extracted randomly flat in the ranges discussed in Section 5. Standard neutrino fluxes have been employed. As previously mentioned, we have four independent asymmetries. Three of them ($A_{\mu e}$, $A_{\mu\mu}$, and $A_{\mu\tau}$) are accessible through the corresponding oscillation channels. The other one, namely

$A_{\mu s}$, can be measured looking at the NC events. Indeed, since the NC interactions are flavor-independent, the number of events in this channel depends on the sum:

$$N_{NC} \propto P(\nu_\mu \to \nu_e) + P(\nu_\mu \to \nu_\mu) + P(\nu_\mu \to \nu_\tau)\,, \tag{26}$$

which, from the unitarity relation, corresponds to $1 - P(\nu_\mu \to \nu_s)$. Thus, the integrated asymmetry

$$A_{NC} = \frac{N_{NC} - \bar{N}_{NC}}{N_{NC} + \bar{N}_{NC}} \tag{27}$$

is closely related to the μs asymmetry.

We present our results in the $(A_{\mu\tau}, A_{\mu e})$ and $(A_{\mu\mu}, A_{NC})$ planes (see Figure 9) for the standard flux. The situation is quite clear: even though the analytic corrections to $A_{\mu e} \sim \mathcal{O}(\lambda)$ and to $A_{\mu\mu,\mu\tau} \sim \mathcal{O}(\lambda^2)$, the relatively large uncertainties do not allow the $3+1$ points to spread outside the error bars.

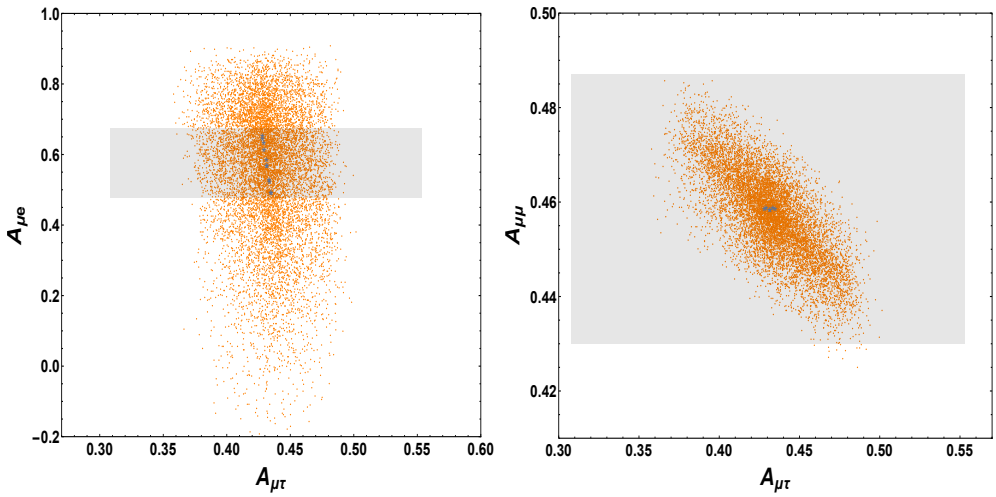

Figure 8. Same as Figure 7 but using the optimized flux.

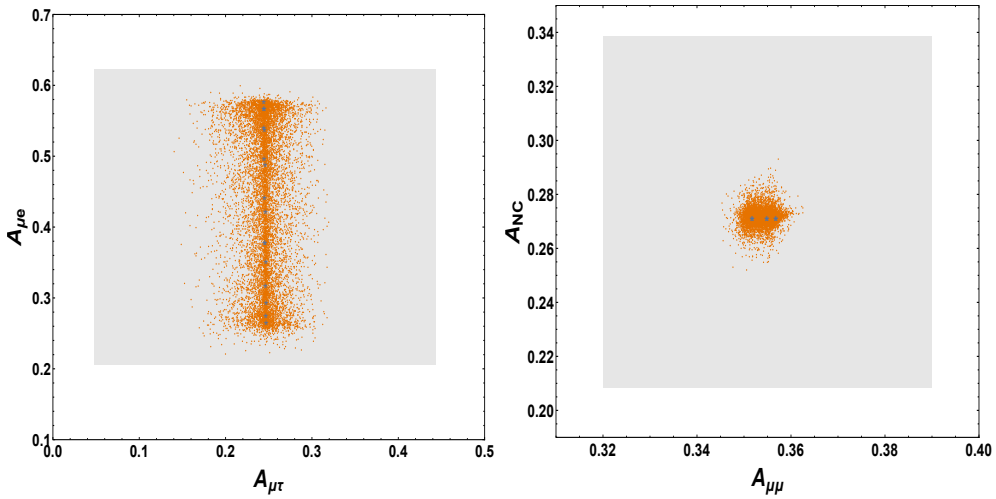

Figure 9. Integrated asymmetries in the $(A_{\mu\tau}, A_{\mu e})$ (**left** plot) and $(A_{\mu\mu}, A_{NC})$ planes (**right** plot) in the sterile neutrino model. The adopted legend for the symbols is the same as for the other plots. Standard neutrino flux has been employed to compute the number of events.

As before, the use of the higher energy flux reduces the error bands and increases the number of points outside the SM uncertainties (see Figure 10). Furthermore, as for the NSI case, the asymmetry that varies the most when NP enters into the game is $A_{\mu e}$ since, as shown in

(20), the correction to SM asymmetry is at first order in our perturbative expansion. It is clear from the left panel of Figure 10 that there are some points at more than two sigmas away from the standard values but, differently from the previous case, $A_{\mu e}$ never becomes negative.

In the $(A_{\mu\mu}, A_{NC})$ plane, no orange point lies outside the grey rectangle.

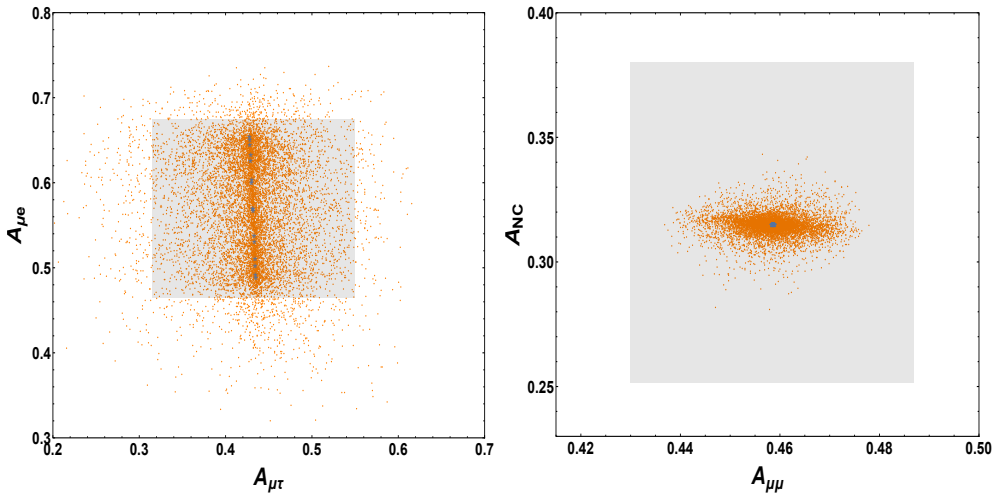

Figure 10. Same as Figure 9 but for the optimized flux.

7. Conclusions

The search for physics beyond the Standard Model has become an attractive research field in the neutrino sector thanks to the huge experimental efforts in the measurement of the standard oscillation parameters. With few exceptions, they are known with good precision and the relevant question is now to establish whether new physics is hidden within the experimental uncertainties. In this respect, the quest for new sources of CP violation beyond the single phase already present in the Standard Model is a pressing one. Contrary to many similar studies in the literature, we avoided focusing on the sensitivity of a given experiment to a particular phase, as many assumptions that are usually made in the fit procedure (marginalization over a subset of parameters while other are kept fixed, and so on) obscure the true sensitivity to CP violation. Instead, we designed a more objective strategy based on the evaluation within the Standard Model of the integrated CP-odd quantities, the asymmetries $A_{\alpha\beta}$, and compare them with the same observables evaluated in the new physics scenarios under consideration. In this paper, we performed a perturbative analytic evaluation of all asymmetries accessible at the DUNE experiment under the assumptions that nonstandard interactions and one sterile state affect the standard neutrino oscillation framework. We then apply our procedure to the more realistic asymmetries built from the expected number of event in DUNE, reaching the conclusion that, for both new physics scenarios, the $A_{\mu e}$ asymmetry can reach values well beyond the Standard Model expectation, including the foreseen statistics and systematic uncertainties, when a high-energy flux is employed. A special mention should be devoted to $A_{\mu\tau}$. While analytic considerations indicate that new physics sets large corrections compared to the Standard Model results, the uncertainties involved in the evaluation of the number of expected events obscure this important feature. An experimental effort should be carried out to reduce the uncertainties in τ detection.

Author Contributions: Conceptualization, A.G. and D.M.; methodology, A.G. and D.M.; software, A.G. and D.M.; validation, A.G. and D.M.; formal analysis, A.G. and D.M.; investigation, A.G. and D.M.; writing—original draft preparation, A.G. and D.M.; writing—review and editing, A.G. and D.M.; visualization, A.G. and D.M.; supervision, A.G. and D.M. All authors have read and agreed to the published version of the manuscript.

Funding: This research received no external funding.

Institutional Review Board Statement: Not applicable.

Informed Consent Statement: Not applicable.

Conflicts of Interest: The authors declare no conflict of interest.

Appendix A. Perturbative Expressions of Probabilities

We provide here the perturbative expressions of the probabilities expanded as discussed in Sections 2–4, in both NSI and the sterile neutrino models. The standard model probabilities can be obtained by putting all new physics parameters to zero.

For the NSI case, we have:

$$\begin{aligned} P(\nu_\mu \to \nu_e)^{NSI} \;=\; & r^2 \sin^2 \Delta_{31} + \frac{4}{3} r\alpha \Delta_{31} (\cos\delta \cos\Delta_{31} - \sin\delta \sin\Delta_{31}) \sin\Delta_{31} + \frac{4}{9}\alpha^2 \Delta_{31}^2 + \\ & +2V_{CC} r \sin\Delta_{31} [\Delta_{31} \cos\Delta_{31} (\varepsilon_{e\mu} \cos(\delta - \delta_{e\mu}) - \varepsilon_{e\tau} \cos(\delta - \delta_{e\tau}) - r) + \\ & +\Delta_{31} \sin\Delta_{31} (\varepsilon_{e\tau} \sin(\delta - \delta_{e\tau}) - \varepsilon_{e\mu} \cos(\delta - \delta_{e\mu}) + \\ & + \sin\Delta_{31} (\varepsilon_{e\mu} \cos(\delta - \delta_{e\mu}) + \varepsilon_{e\tau} \cos(\delta - \delta_{e\tau}) + r)] \end{aligned} \tag{A1}$$

$$\begin{aligned} P(\nu_\mu \to \nu_\mu)^{NSI} \;=\; & \cos^2 \Delta_{31} + \frac{4}{3}\alpha \Delta_{31} \sin\Delta_{31} \cos\Delta_{31} - \frac{4}{9}\alpha^2 \Delta_{31}^2 (2 - 3\sin^2 \Delta_{31}) + \\ & -\frac{4}{3} r\alpha \cos\delta \cos\Delta_{31} \sin\Delta_{31} + 4a^2 \sin\Delta_{31} - \frac{4}{3} s\alpha \Delta_{31} \sin\Delta_{31} \cos\Delta_{31} + \\ & +V_{CC} \Big\{ -8\Delta_{31} \varepsilon_{\mu\tau} \cos\delta_{\mu\tau} \cos\Delta_{31} \sin\Delta_{31} + \frac{4}{3}\alpha \Delta_{31}^2 [r \cos\delta \cos^2 \Delta_{31} + \\ & -\varepsilon_{e\mu} \cos\delta_{e\mu} \cos^2 \Delta_{31} + \varepsilon_{e\tau} \cos\delta_{e\tau} \cos^2 \Delta_{31} + 4\varepsilon_{\mu\tau} \cos\delta_{\mu\tau} (1 - 2\sin^2 \Delta_{31})] + \\ & +4a\Delta_{31} \varepsilon_{\tau\tau} \cos\Delta_31 \sin\Delta_{31} \} + 4r\Delta_{31} \varepsilon_{e\mu} \cos(\delta - \delta_{e\mu}) \cos\Delta_{31} \sin\Delta_{31} + \\ & -4a\varepsilon_{\tau\tau} \sin^2 \Delta_{31} + \frac{4}{3}\alpha \Delta_{31} [\varepsilon_{e\tau} \cos\delta_{e\tau} \cos\Delta_{31} \sin\Delta_{31} + \\ & -\varepsilon_{e\mu} \cos\delta_{e\mu} \cos\Delta_{31} \sin\Delta_{31} - r \cos\delta \cos\Delta_{31} \sin\Delta_{31}] \Big\} \end{aligned} \tag{A2}$$

$$\begin{aligned} P(\nu_\mu \to \nu_\tau)^{NSI} \;=\; & \sin^2 \Delta_{31} - \frac{4}{3}\alpha \Delta_{31} \cos\Delta_{31} \sin\Delta_{31} + \\ & -\frac{4}{9}\alpha^2 \Delta_{31}^2 (3\sin^2 \Delta_{31} - 2) - 4a^2 \sin^3 \Delta_{31} - r^2 \sin^2 \Delta_{31} + \\ & -\frac{4}{3}\alpha \Delta_{31} \sin\Delta_{31} (s \cos\Delta_{31} + r \sin\delta' \sin\Delta_{31}) + \\ & +2V_{CC} \Big[4\Delta_{31} \varepsilon_{\mu\tau} \cos\delta_{\mu\tau} \sin\Delta_{31} \cos\Delta_{31} + r^2 \sin\Delta_{31} (\Delta_{31} \cos\Delta_{31} + \\ & - \sin\Delta_{31}) + \frac{4}{27}\alpha^2 \Delta_{31}^2 \cos\Delta_{31} \Delta_{31} + \frac{2}{3} r\alpha \sin\delta \sin\Delta_{31} (\sin\Delta_{31} - \Delta_{31} \cos\Delta_{31}) + \\ & -\frac{8}{3}\alpha \Delta_{31}^2 \varepsilon_{\mu\tau} \cos\delta_{\mu\tau} (1 - 2\sin^2 \Delta_{31}) + \frac{2}{3} a\Delta_{31} \varepsilon_{e\mu} \sin\delta_{e\mu} \sin^2 \Delta_{31} + \\ & -2a\varepsilon_{\tau\tau} \sin\Delta_{31} (\Delta_{31} \cos\Delta_{31} - \sin\Delta_{31}) + \frac{2}{3}\alpha \Delta_{31} \varepsilon_{e\tau} \sin^2 \Delta_{31} (\sin\delta_{e\tau} + \Delta_{31} \cos\delta_{e\tau}) + \\ & +\frac{2}{3}\alpha \Delta_{31} \varepsilon_{e\mu} \sin^2 \Delta_{31} (\sin\delta_{e\mu} - \Delta_{31} \cos\delta_{e\mu}) + r\Delta_{31} \varepsilon_{e\mu} \cos(\delta - \delta_{e\mu}) \sin\Delta_{31} \cos\Delta_{31} + \\ & -r\varepsilon_{e\mu} \sin^2 \Delta_{31} (\cos(\delta - \delta_{e\mu}) - \Delta_{31} \sin(\delta - \delta_{e\mu})) + \\ & +r\Delta_{31} \varepsilon_{e\tau} \cos(\delta - \delta_{e\mu}) \cos\Delta_{31} \sin\Delta_{31} + \\ & +r\varepsilon_{e\tau} \sin^2 \Delta_{31} (\cos(\delta - \delta_{e\tau}) - \Delta_{31} \sin(\delta - \delta_{e\tau})) \Big] \end{aligned} \tag{A3}$$

For the $3+1$ model, we found the following expressions ($\delta' = \delta_2 - \delta_1 - \delta_3$):

$$\begin{aligned} P(\nu_\mu \to \nu_e)^{3+1} &= r^2 \sin^2 \Delta_{31} + \frac{4}{3} r\alpha\Delta_{31}(\cos\delta' \cos\Delta_{31} - \sin\delta' \sin\Delta_{31}) \sin\Delta_{31} + \frac{4}{9}\alpha^2\Delta_{31}^2 + \\ & V_{CC}\Big[-2r^2 \sin^2\Delta_{31} - 2r^2\Delta_{31}\cos\Delta_{31}\sin\Delta_{31} + \\ & + \frac{4}{3} r\alpha\Delta_{31}(\cos\delta'\cos\Delta_{31} - \sin\delta'\sin\Delta_{31})(\sin\Delta_{31} - \Delta_{31}\cos\Delta_{31})\Big] \end{aligned} \tag{A4}$$

$$\begin{aligned} P(\nu_\mu \to \nu_\mu)^{3+1} &= (1 - 2s_{24}^2)\cos^2\Delta_{31} + \frac{4}{3}\alpha\Delta_{31}\sin\Delta_{31}\cos\Delta_{31} - \frac{4}{9}\alpha^2\Delta_{31}^2(2 - 3\sin^2\Delta_{31}) + \\ & -\frac{4}{3} r\alpha\cos\delta'\cos\Delta_{31}\sin\Delta_{31} + 4a^2\sin\Delta_{31} - \frac{4}{3} s\alpha\Delta_{31}\sin\Delta_{31}\cos\Delta_{31} + \\ & + \frac{4}{27}\alpha\Delta_{31} V_{CC}[9r\cos\delta'\cos\Delta_{31}(\Delta_{31}\cos\Delta_{31} - \sin\Delta_{31} + \\ & -2\alpha\Delta_{31}^2\sin\Delta_{31}\cos\Delta_{31}] + 4V_{NC}\Delta_{31}s_{24}s_{34}\cos\delta_3\cos\Delta_{31}\sin\Delta_{31} \end{aligned} \tag{A5}$$

$$\begin{aligned} P(\nu_\mu \to \nu_\tau)^{3+1} &= \sin^2\Delta_{31} - \frac{4}{3}\alpha\Delta_{31}\cos\Delta_{31}\sin\Delta_{31} + \\ & -\frac{4}{9}\alpha^2\Delta_{31}^2(3\sin^2\Delta_{31} - 2) - 4a^2\sin^3\Delta_{31} - r^2\sin^2\Delta_{31} + \\ & -\frac{4}{3}\alpha\Delta_{31}\sin\Delta_{31}(s\cos\Delta_{31} + r\sin\delta'\sin\Delta_{31}) + (s_{24}^2 - s_{34}^2)\sin^2\Delta_{31} + \\ & +2s_{24}s_{34}\sin\delta_3\sin\Delta_{31}\cos\Delta_{31} + V_{CC}\Big[2r^2\sin\Delta_{31}(\Delta_{31}\cos\Delta_{31} - \sin\Delta_{31}) + \\ & + \frac{8}{27}\alpha^2\Delta_{31}^3\cos\Delta_{31}\sin\Delta_{31} - \frac{4}{3} r\alpha\Delta_{31}\sin\delta'\sin\Delta_{31}(\Delta_{31}\cos\Delta_{31} - \sin\Delta_{31})\Big] + \\ & -4V_{NC}s_{24}s_{34}\cos\delta_3\cos\Delta_{31}\sin\Delta_{31} \end{aligned} \tag{A6}$$

$$P(\nu_\mu \to \nu_s)^{3+1} = s_{24}^2(2 - \sin^2\Delta_{31}) + s_{34}^2\sin^2\Delta_{31} - 2s_{24}s_{34}\sin\delta_3\cos\Delta_{31}\sin\Delta_{31} \tag{A7}$$

Appendix B. Probabilities in the $3+1$ Model for Not-Averaged Δm_{41}^2

In this appendix, we will provide the perturbative expressions for the asymmetries in the $3+1$ model in the case that the oscillations driven by Δm_{41}^2 cannot be averaged out. The leading order of $A_{\mu e}$ is unchanged; thus, there are no corrections to the SM at the chosen perturbative order.

For the other asymmetries, we give a first order expansion in the matter potentials V_{CC} and V_{NC} here. Thus, we put the corrections in the following form:

$$A_{\alpha\beta}^{3+1} = (A_{\alpha\beta}^{3+1})_0 + V_{CC}(A_{\alpha\beta}^{3+1})_{CC} + V_{NC}(A_{\alpha\beta}^{3+1})_{NC} + \mathcal{O}(V^2, \lambda^3)\,. \tag{A8}$$

For the $\mu\tau$ asymmetry, we have:

$$\begin{aligned} (A_{\mu\tau}^{3+1})_0 &= A_{\mu\tau}^{SM_0} + 4s_{24}s_{34}\sin\delta_3(\cot\Delta_{31}\sin^2\Delta_{41} + \sin\Delta_{41}\cos\Delta_{41}) \\ (A_{\mu\tau}^{3+1})_{CC} &= A_{\mu\tau}^{SM_1} \\ (A_{\mu\tau}^{3+1})_{NC} &= s_{24}^2 b_{\mu\tau}^{s_{24}^2} + s_{34}^2 b_{\mu\tau}^{s_{34}^2} + s_{24}s_{34} b_{\mu\tau}^{s_{24}s_{34}} \end{aligned} \tag{A9}$$

where $\Delta_{41} = \Delta m^2_{41} L/E_\nu$ and:

$$
\begin{aligned}
b_{\mu\tau}^{s_{24}^2} &= \frac{2\Delta_{41} - 2\Delta_{31}(\sin^2\Delta_{31} + \cot\Delta_{31}\sin\Delta_{41}\cos\Delta_{41})}{(\Delta_{41}/\Delta_{31})(\Delta_{31}-\Delta_{41})} && \text{(A10)}\\
b_{\mu\tau}^{s_{34}^2} &= b_{\mu\tau}^{s_{24}^2} && \text{(A11)}\\
b_{\mu\tau}^{s_{24}s_{34}} &= -8\cos\delta_3(\cot\Delta_{31}\cos^2\Delta_{41} + \sin\Delta_{41}\cos\Delta_{41}) + \\
&\quad +2\cos\delta_3\Delta_{31}\frac{2\sin^2\Delta_{41} - \cot\Delta_{31}\sin\Delta_{41}\cos\Delta_{41}}{(\Delta_{41}/\Delta_{31})(\Delta_{31}-\Delta_{41})} + \\
&\quad +4\cos\delta_3\Delta_{41}\frac{1 - 2\sin^2\Delta_{41} + \cot\Delta_{31}\sin\Delta_{41}\cos\Delta_{41}}{(\Delta_{41}/\Delta_{31})(\Delta_{31}-\Delta_{41})} && \text{(A12)}
\end{aligned}
$$

For the $\mu\mu$ asymmetry:

$$
\begin{aligned}
(A_{\mu\mu}^{3+1})_0 &= 0 \\
(A_{\mu\mu}^{3+1})_{CC} &= A_{\mu\mu}^{SM_1} && \text{(A13)}\\
(A_{\mu\mu}^{3+1})_{NC} &= s_{24}^2 b_{\mu\mu}^{s_{24}^2} + s_{24}s_{34} b_{\mu\mu}^{s_{24}s_{34}}
\end{aligned}
$$

where

$$
\begin{aligned}
b_{\mu\mu}^{s_{24}^2} &= -4\Delta_{31}[\tan\Delta_{31}(1 - 2\sin^2\Delta_{41}) - 2\sin\Delta_{41}\cos\Delta_{41}] + \\
&\quad \frac{4(\Delta_{31} - 2\Delta_{41})}{(\Delta_{41}/\Delta_{31})(\Delta_{31}-\Delta_{41})}(\tan\Delta_{31}\sin\Delta_{41}\cos\Delta_{41} - \sin^2\Delta_{41}) && \text{(A14)}\\
b_{\mu\mu}^{s_{24}s_{34}} &= 4\Delta_{31}\cos\delta_3\tan\Delta_{31} + 4\cos\delta_3\Delta_{31}\frac{\sin^2\Delta_{41} + \tan\Delta_{31}\sin\Delta_{41}\cos\Delta_{41}}{(\Delta_{41}/\Delta_{31})(\Delta_{41}-\Delta_{31})} && \text{(A15)}
\end{aligned}
$$

Finally, for the μs asymmetry, we found:

$$
\begin{aligned}
(A_{\mu s}^{3+1})_0 &= \frac{4s_{24}s_{34}\sin\delta_3(\sin\Delta_{41}\cos\Delta_{41}\sin^2\Delta_{31} - \sin\Delta_{31}\cos\Delta_{31}\sin^2\Delta_{41})}{d_0} \\
(A_{\mu s}^{3+1})_{CC} &= 0 && \text{(A16)}\\
(A_{\mu s}^{3+1})_{NC} &= \frac{s_{24}^3 s_{34} b_{\mu s}^{s_{24}^3 s_{34}} + s_{34}^3 s_{24} b_{\mu s}^{s_{34}^3 s_{24}} + s_{24}^2 s_{34}^2 b_{\mu s}^{s_{24}^2 s_{34}^2}}{s_{24}^3 s_{34} d_{\mu s}^{s_{24}^3 s_{34}} + s_{34}^3 s_{24} d_{\mu s}^{s_{34}^3 s_{24}} + s_{24}^2 s_{34}^2 d_{\mu s}^{s_{24}^2 s_{34}^2}}
\end{aligned}
$$

where

$$
\begin{aligned}
d_0 &= (s_{34}^2 - s_{24}^2)\sin^2\Delta_{31} + \\
&\quad +2s_{24}^2(\sin^2\Delta_{31} + 2\sin^2\Delta_{41}\cos^2\Delta_{31} + 2\sin\Delta_{31}\cos\Delta_{31}\sin\Delta_{41}\cos\Delta_{41}) + \\
&\quad +2s_{24}s_{34}\cos\delta_3\sin\Delta_{31}[\sin\Delta_{31}(1 - 2\sin^2\Delta_{41}) - 2\cos\Delta_{31}\sin\Delta_{41}\cos\Delta_{41}] && \text{(A17)}
\end{aligned}
$$

and the $b_{\mu s}$ and $d_{\mu s}$ are complicated functions that, in the limit $\Delta_{41} \gg \Delta_{31}$ can be reduced to

$$
\begin{aligned}
b_{\mu s}^{s_{24}^3 s_{34}} &= 0 \\
b_{\mu s}^{s_{34}^3 s_{24}} &= 2\Delta_{31}\cos\delta_3 \sin^2\Delta_{31}(1-2\sin^2\Delta_{41}) \\
b_{\mu s}^{s_{34}^2 s_{24}^2} &= 4\Delta_{31}\sin\Delta_{31}\cos\Delta_{41}\sin\Delta_{41}(4\sin^2\Delta_{41}-3) \\
d_{\mu s}^{s_{24}^3 s_{34}} &= 4\cos\delta_3\sin\Delta_{41}\cos\Delta_{41}(\sin^2\Delta_{31}-4\sin^2\Delta_{41}) \\
d_{\mu s}^{s_{34}^3 s_{24}} &= -2\cos\delta_3\sin^2\Delta_{31}\sin\Delta_{41}\cos\Delta_{41} \\
d_{\mu s}^{s_{34}^2 s_{24}^2} &= \sin\Delta_{31}(4\sin^2\Delta_{41}+8\sin^2\Delta_{41}\cos^2\Delta_{41}\cos^2\delta_3-\sin^2\Delta_{31})
\end{aligned}
\tag{A18}
$$

References

1. Fukuda, Y.; et al. [Super-Kamiokande]. Evidence for Oscillation of Atmospheric Neutrinos. *Phys. Rev. Lett.* **1998**, *81*, 1562–1567. [CrossRef]
2. Esteban, I.; Gonzalez-Garcia, M.C.; Maltoni, M.; Schwetz, T.; Zhou, A. The fate of hints: Updated global analysis of three-flavor neutrino oscillations. *J. High Energy Phys.* **2020**, *178*, 9. [CrossRef]
3. De Salas, P.F.; Forero, D.V.; Gariazzo, S.; Martínez-Miravé, P.; Mena, O.; Ternes, C.A.; Tórtola, M.; Valle, J.W.F.2020 global reassessment of the neutrino oscillation picture. *J. High Energy Phys.* **2021**, *2*, 71. [CrossRef]
4. Kolupaeva, L. [NOvA]. Recent three-flavor neutrino oscillation results from the NOvA experiment. *J. Phys. Conf. Ser.* **2020**, *1690*, 012172. [CrossRef]
5. Abe, K.; et al. [T2K]. Improved constraints on neutrino mixing from the T2K experiment with $\mathbf{3.13 \times 10^{21}}$ protons on target. *arXiv* **2021**, arXiv:2101.03779.
6. Athanassopoulos, C.; et al. [LSND]. Candidate events in a search for anti-muon-neutrino —> anti-electron-neutrino oscillations. *Phys. Rev. Lett.* **1995**, *75*, 2650–2653. [CrossRef]
7. Aguilar-Arevalo, A.; et al. [LSND]. Evidence for neutrino oscillations from the observation of $\bar{\nu}_e$ appearance in a $\bar{\nu}_\mu$ beam. *Phys. Rev. D* **2001**, *64*, 112007. [CrossRef]
8. Aguilar-Arevalo, A.A.; et al. [MiniBooNE]. Significant Excess of ElectronLike Events in the MiniBooNE Short-Baseline Neutrino Experiment. *Phys. Rev. Lett.* **2018**, *121*, 221801. [CrossRef]
9. Mention, G.; Fechner, M.; Lasserre, T.; Mueller, T.A.; Lhuillier, D.; Cribier, M.; Letourneau, A. The Reactor Antineutrino Anomaly. *Phys. Rev. D* **2011**, *83*, 073006. [CrossRef]
10. Giunti, C.; Li, Y.F.; Littlejohn, B.R.; Surukuchi, P.T. Diagnosing the Reactor Antineutrino Anomaly with Global Antineutrino Flux Data. *Phys. Rev. D* **2019**, *99*, 073005. [CrossRef]
11. Berryman, J.M.; Huber, P. Reevaluating Reactor Antineutrino Anomalies with Updated Flux Predictions. *Phys. Rev. D* **2020**, *101*, 015008. [CrossRef]
12. Berryman, J.M.; Huber, P. Sterile Neutrinos and the Global Reactor Antineutrino Dataset. *J. High Energy Phys.* **2021**, *1*, 167. [CrossRef]
13. Agarwalla, S.K.; Chatterjee, S.S.; Dasgupta, A.; Palazzo, A. Discovery Potential of T2K and NOvA in the Presence of a Light Sterile Neutrino. *J. High Energy Phys.* **2016**, *1602*, 111. [CrossRef]
14. Agarwalla, S.K.; Chatterjee, S.S.; Palazzo, A. Physics Reach of DUNE with a Light Sterile Neutrino. *J. High Energy Phys.* **2016**, *1609*, 16. [CrossRef]
15. Dutta, D.; Gandhi, R.; Kayser, B.; Masud, M.; Prakash, S. Capabilities of long-baseline experiments in the presence of a sterile neutrino. *J. High Energy Phys.* **2016**, *1611*, 122. [CrossRef]
16. Adamson, P.; et al. [NOvA Collaboration]. Search for active-sterile neutrino mixing using neutral-current interactions in NOvA. *Phys. Rev. D* **2017**, *96*, 072006. [CrossRef]
17. Adamson, P.; et al. [MINOS+ Collaboration]. Search for sterile neutrinos in MINOS and MINOS+ using a two-detector fit. *Phys. Rev. Lett.* **2019**, *122*, 091803. [CrossRef]
18. Choubey, S.; Dutta, D.; Pramanik, D. Measuring the Sterile Neutrino CP Phase at DUNE and T2HK. *Eur. Phys. J. C* **2018**, *78*, 1–14. [CrossRef]
19. Agarwalla, S.K.; Chatterjee, S.S.; Palazzo, A. Signatures of a Light Sterile Neutrino in T2HK. *J. High Energy Phys.* **2018**, *2018*, 1–22. [CrossRef]
20. Gupta, S.; Matthews, Z.M.; Sharma, P.; Williams, A.G. The Effect of a Light Sterile Neutrino at NOνA and DUNE. *Phys. Rev. D* **2018**, *98*, 035042. [CrossRef]
21. Böser, S.; Buck, C.; Giunti, C.; Lesgourgues, J.; Ludhova, L.; Mertens, S.; Schukraft, A.; Wurm, M. Status of Light Sterile Neutrino Searches. *Prog. Part. Nucl. Phys.* **2020**, *111*, 103736. [CrossRef]
22. Dentler, M.; Hernández-Cabezudo, J.; Kopp, J.; Machado, P.A.N.; Maltoni, M.; Martinez-Soler, I.; Schwetz, T. Updated Global Analysis of Neutrino Oscillations in the Presence of eV-Scale Sterile Neutrinos. *J. High Energy Phys.* **2018**, *2018*, 1–35. [CrossRef]

23. Thakore, T.; Devi, M.M.; Agarwalla, S.K.; Dighe, A. Active-sterile neutrino oscillations at INO-ICAL over a wide mass-squared range. *J. High Energy Phys.* **2018**, *2018*, 1–34. [CrossRef]
24. Abe, K.; et al. [T2K Collaboration]. Search for light sterile neutrinos with the T2K far detector Super-Kamiokande at a baseline of 295 km. *Phys. Rev. D* **2019**, *99*, 071103. [CrossRef]
25. Roulet, E. MSW effect with flavor changing neutrino interactions. *Phys. Rev. D* **1991**, *44*, 935.
26. Kopp, J.; Lindner, M.; Ota, T.; Sato, J. Non-standard neutrino interactions in reactor and superbeam experiments. *Phys. Rev. D* **2008**, *77*, 013007. [CrossRef]
27. Guzzo, M.M.; Masiero, A.; Petcov, S.T. On the MSW effect with massless neutrinos and no mixing in the vacuum. *Phys. Lett. B* **1991**, *260*, 154. [CrossRef]
28. Farzan, Y.; Tortola, M. Neutrino oscillations and Non-Standard Interactions. *Front. Phys.* **2018**, *6*, 10. [CrossRef]
29. Masud, M.; Chatterjee, A.; Mehta, P. Probing CP violation signal at DUNE in presence of non-standard neutrino interactions. *J. Phys. G* **2016**, *43*, 095005. [CrossRef]
30. Esteban, I.; Gonzalez-Garcia, M.C.; Maltoni, M. On the Determination of Leptonic CP Violation and Neutrino Mass Ordering in Presence of Non-Standard Interactions: Present Status. *J. High Energy Phys.* **2019**, *6*, 55. [CrossRef]
31. De Gouvêa, A.; Kelly, K.J. Non-standard Neutrino Interactions at DUNE. *Nucl. Phys. B* **2016**, *908*, 318. [CrossRef]
32. Coloma, P. Non-Standard Interactions in propagation at the Deep Underground Neutrino Experiment. *J. High Energy Phys.* **2016**, *1603*, 16. [CrossRef]
33. Huitu, K.; Kärkkäinen, T.J.; Maalampi, J.; Vihonen, S. Constraining the nonstandard interaction parameters in long baseline neutrino experiments. *Phys. Rev. D* **2016**, *93*, 053016. [CrossRef]
34. Dev, P.S.B.; Babu, K.S.; Denton, P.B.; Machado, P.A.N.; Argüelles, C.A.; Barrow, J.L.; Chatterjee, S.S.; Chen, M.C.; de Gouvêa, A.; Dutta, B.; et al. Neutrino Non-Standard Interactions: A Status Report. *SciPost Phys. Proc.* **2019**, *2*, 1. [CrossRef]
35. Masud, M.; Mehta, P. Nonstandard interactions spoiling the CP violation sensitivity at DUNE and other long baseline experiments. *Phys. Rev. D* **2016**, *94*, 013014. [CrossRef]
36. Blennow, M.; Choubey, S.; Ohlsson, T.; Pramanik, D.; Raut, S.K. A combined study of source, detector and matter non-standard neutrino interactions at DUNE. *J. High Energy Phys.* **2016**, *1608*, 90. [CrossRef]
37. Fukasawa, S.; Ghosh, M.; Yasuda, O. Sensitivity of the T2HKK experiment to nonstandard interactions. *Phys. Rev. D* **2017**, *95*, 055005. [CrossRef]
38. Liao, J.; Marfatia, D.; Whisnant, K. Nonstandard neutrino interactions at DUNE, T2HK and T2HKK. *J. High Energy Phys.* **2017**, *1701*, 71. [CrossRef]
39. Verma, S.; Bhardwaj, S. Non-standard interactions and parameter degeneracies in DUNE and T2HKK. *arXiv* **2018**, arXiv:1808.04263.
40. Altarelli, G.; Meloni, D. CP violation in neutrino oscillations and new physics. *Nucl. Phys. B* **2009**, *809*, 158–182. [CrossRef]
41. Acciarri, R.; et al. [DUNE Collaboration]. Long-Baseline Neutrino Facility (LBNF) and Deep Underground Neutrino Experiment (DUNE): Conceptual Design Report, Volume 1: The LBNF and DUNE Projects. *arXiv* **2016**, arXiv:1601.05471.
42. Acciarri, R.; et al. [DUNE Collaboration]. Long-Baseline Neutrino Facility (LBNF) and Deep Underground Neutrino Experiment (DUNE) : Conceptual Design Report, Volume 2: The Physics Program for DUNE at LBNF. *arXiv* **2015**, arXiv:1512.06148.
43. Abi, B.; et al. [DUNE Collaboration]. Deep Underground Neutrino Experiment (DUNE), Far Detector Technical Design Report, Volume I Introduction to DUNE. *arXiv* **2020**, arXiv:2002.02967.
44. Abi, B.; et al. [DUNE Collaboration]. Deep Underground Neutrino Experiment (DUNE), Far Detector Technical Design Report, Volume II DUNE Physics. *arXiv* **2020**, arXiv:2002.03005.
45. Donini, A.; Gavela, M.B.; Hernandez, P.; Rigolin, S. Neutrino mixing and CP violation. *Nucl. Phys. B* **2000**, *574*, 23–42. [CrossRef]
46. King, S.F. Parametrizing the lepton mixing matrix in terms of deviations from tri-bimaximal mixing. *Phys. Lett. B* **2008**, *659*, 244–251. [CrossRef]
47. Pakvasa, S.; Rodejohann, W.; Weiler, T.J. Unitary parametrization of perturbations to tribimaximal neutrino mixing. *Phys. Rev. Lett.* **2008**, *100*, 111801. [CrossRef]
48. Miranda, O.G.; Tortola, M.A.; Valle, J.W.F. Are solar neutrino oscillations robust? *J. High Energy Phys.* **2006**, *10*, 8. [CrossRef]
49. Maltoni, M.; Schwetz, T. Sterile neutrino oscillations after first MiniBooNE results. *Phys. Rev. D* **2007**, *76*, 093005. [CrossRef]
50. Donini, A.; Maltoni, M.; Meloni, D.; Migliozzi, P.; Terranova, F. 3+1 sterile neutrinos at the CNGS. *J. High Energy Phys.* **2007**, *712*, 13. [CrossRef]
51. Meloni, D.; Tang, J.; Winter, W. Sterile neutrinos beyond LSND at the Neutrino Factory. *Phys. Rev. D* **2010**, *82*, 093008. [CrossRef]
52. Rout, J.; Masud, M.; Mehta, P. Can we probe intrinsic CP and T violations and nonunitarity at long baseline accelerator experiments?. *Phys. Rev. D* **2017**, *95*, 075035. [CrossRef]
53. Masud, M.; Bishai, M.; Mehta, P. Extricating New Physics Scenarios at DUNE with Higher Energy Beams. *Sci. Rep.* **2019**, *9*, 352. [CrossRef]
54. Masud, M.; Roy, S.; Mehta, P. Correlations and degeneracies among the NSI parameters with tunable beams at DUNE. *Phys. Rev. D* **2019**, *99*, 115032. [CrossRef]
55. Available online: http://home.fnal.gov/~ljf26/DUNEFluxes/ (accessed on 2 June 2021)

56. Bishai, M.; Dolce, M. Optimization of the LBNF/DUNE Beamline for Tau Neutrinos, in Document Database (DocDB) for DUNE and LBNF. Available online: http://docs.dunescience.org/cgi-bin/RetrieveFile?docid=2013&filename=DOLCE_M_report.pdf&version=1 (accessed on 2 June 2021).
57. Huber, P.; Lindner, M.; Winter, W. Simulation of long-baseline neutrino oscillation experiments with GLoBES (General Long Baseline Experiment Simulator). *Comput. Phys. Commun.* **2005**, *167*, 195. [CrossRef]
58. Huber, P.; Kopp, J.; Lindner, M.; Rolinec, M.; Winter, W. New features in the simulation of neutrino oscillation experiments with GLoBES 3.0: General Long Baseline Experiment Simulator. *Comput. Phys. Commun.* **2007**, *177*, 432. [CrossRef]
59. Alion, T.; et al. [DUNE]. Experiment Simulation Configurations Used in DUNE CDR. *arXiv* **2016**, arXiv:1606.09550.
60. Abi, B.et al. [DUNE]. Experiment Simulation Configurations Approximating DUNE TDR. *arXiv* **2021**, arXiv:2103.04797.
61. Gouvêa, A.D.; Kelly, K.J.; Stenico, G.; Pasquini, P. Physics with Beam Tau-Neutrino Appearance at DUNE. *Phys. Rev. D* **2019**, *100*, 016004. [CrossRef]
62. Ghoshal, A.; Giarnetti, A.; Meloni, D. On the role of the ν_τ appearance in DUNE in constraining standard neutrino physics and beyond. *J. High Energy Phys.* **2019**, *12*, 126. [CrossRef]
63. Coloma, P.; Forero, D.V.; Parke, S.J. DUNE Sensitivities to the Mixing between Sterile and Tau Neutrinos. *J. High Energy Phys.* **2018**, *1807*, 79. [CrossRef]